The Voltage Dependence of a Cloned Mammalian Renal Type II Na^+/P_i Cotransporter (NaP_i-2)

Ian Forster, Nati Hernando, Jürg Biber, and Heini Murer

From the Physiologisches Institut, Universität Zürich, CH-8057 Zürich, Switzerland

ABSTRACT The voltage dependence of the rat renal type II Na^+/P_i cotransporter (NaP_i-2) was investigated by expressing NaP_i-2 in *Xenopus laevis* oocytes and applying the two-electrode voltage clamp. In the steady state, superfusion with inorganic phosphate (P_i) induced inward currents (I_p) in the presence of 96 mM Na^+ over the potential range $-140 \leq V \leq +40$ mV. With P_i as the variable substrate, the apparent affinity constant (K_m^{Pi}) was strongly dependent on Na^+, increasing sixfold for a twofold reduction in external Na^+. K_m^{Pi} increased with depolarizing voltage and was more sensitive to voltage at reduced Na^+. The Hill coefficient was close to unity and the predicted maximum I_p (I_{pmax}) was 40% smaller at 50 mM Na^+. With Na^+ as the variable substrate, K_m^{Na} was weakly dependent on both P_i and voltage, the Hill coefficient was close to 3 and I_{pmax} was independent of P_i at -50 mV. The competitive inhibitor phosphonoformic acid suppressed the steady state holding current in a Na^+-dependent manner, indicating the existence of uncoupled Na^+ slippage. Voltage steps induced pre–steady state relaxations typical for Na^+-coupled cotransporters. NaP_i-2-dependent relaxations were quantitated by a single, voltage-dependent exponential. At 96 mM Na^+, a Boltzmann function was fit to the steady state charge distribution (Q-V) to give a midpoint voltage ($V_{0.5}$) in the range -20 to -50 mV and an apparent valency of ~ 0.5 e^-. $V_{0.5}$ became more negative as Na^+ was reduced. P_i suppressed relaxations in a dose-dependent manner, but had little effect on their voltage dependence. Reducing external pH shifted $V_{0.5}$ to depolarizing potentials and suppressed relaxations in the absence of Na^+, suggesting that protons interact with the unloaded carrier. These findings were incorporated into an ordered kinetic model whereby Na^+ is the first and last substrate to bind, and the observed voltage dependence arises from the unloaded carrier and first Na^+ binding step.

KEY WORDS: ion cotransport • kinetics • steady state • pre–steady state relaxations • *Xenopus laevis* oocytes

INTRODUCTION

The reabsorption of inorganic phosphate (P_i)[1] at the epithelial brush border membrane lining the proximal tubule lumen of the mammalian kidney is the result of a secondary active transport process. This is mediated by a substrate-specific, cotransporter protein that couples a downhill Na^+ flux to inward transport of P_i (reviewed in Murer et al., 1991, 1994; Murer and Biber, 1997). Two renal P_i cotransporter types have been identified so far. The type II Na^+/P_i cotransporter is distinguished from the type I both at the molecular level and functionally by its higher P_i affinity, sensitivity to pH, regulation by external P_i, and strong dependence on external Na^+ (Murer and Biber, 1997). Moreover, under physiological conditions, type II Na^+/P_i transport kinetics are electrogenic, whereby each transport cycle involves a net transmembrane charge transfer (Busch et al., 1994). As a consequence of electrogenicity, if any step in the transport cycle carries charge across the membrane, then that step must be sensitive to the membrane potential, thereby giving rise to voltage-dependent kinetics.

Evidence for electrogenic Na^+/P_i cotransport was first reported by Hoffmann et al. (1976) and later confirmed by Béliveau and co-workers (Béliveau and Ibnoul-Khatib, 1988; Béliveau and Strévey, 1991) using tracer flux techniques applied to isolated renal brush border membrane vesicles (BBMVs). Furthermore, Burkhardt et al. (1981) demonstrated that P_i induced a change in membrane potential by preloading vesicles with a voltage-sensitive fluorescent dye. However, in all these studies the lack of direct control of the BBMV transmembrane potential has prevented precise characterization of the electrogenicity of Na^+/P_i cotransport.

Direct evidence for electrogenicity was obtained from microelectrode studies on intact proximal tubules, whereby addition of P_i to the luminal perfusate caused a depolarization of the epithelial membrane (Samarzija et al., 1980), consistent with a net inward

Portions of this work were previously published in abstract form (Forster, I., A.E. Busch, F. Lang, J. Biber, and H. Murer. 1996. *J. Am. Soc. Nephrol.* 7:*A*2769; Forster, I., A.E. Busch, F. Lang, J. Biber, and H. Murer. 1996. *J. Am. Soc. Nephrol.* 7:*A*2770).

Address correspondence to Dr. Ian C. Forster, Physiologisches Institut, Universität Zürich, Winterthurerstrasse 190, CH-8057 Zürich, Switzerland. Fax: +41 1 635 6814; E-mail: forster@physiol.unizh.ch

[1]*Abbreviations used in this paper:* BBMV, brush border membrane vesicles; I_h, oocyte holding current; I_p, P_i-induced inward currents; I_{PFA}, PFA-sensitive component; I-V, current–voltage; NaP_i-2 rat type II Na^+/P_i cotransporter; PFA, phosphonoformic acid; P_i, inorganic phosphate; V_h, oocyte holding potential.

J. Gen. Physiol. © The Rockefeller University Press • 0022-1295/98/07/1/18 $2.00
Volume 112 July 1998 1–18
http://www.jgp.org

flux of positive charge. More recently, Busch et al. (1994) characterized the electrogenicity by expressing the type II Na^+/P_i cotransporter (NaP_i-2), cloned from rat kidney in *Xenopus laevis* oocytes. They showed that in the mandatory presence of extracellular Na^+, P_i induced an inward current (I_p) for membrane potentials (V) in the range $-80 < V < +10$ mV. Consistent with the findings from BBMVs, the magnitude of I_p depended on the substrate concentrations, the extracellular pH, and membrane potential. However, in contrast to the 2:1 stoichiometry for Na^+/P_i at pH 7.4 proposed from BBMV studies, a finding of a Hill slope close to 3 for the Na^+ dose response at saturating P_i suggested a 3:1 stoichiometry for type II Na^+/P_i cotransport at -50 mV.

To develop comprehensive kinetic models of type II Na^+/P_i cotransport, account must be taken of the modulation of transport function by membrane potential, thereby necessitating identification of voltage-dependent partial reactions in the transport cycle. We now address this need by characterizing both the steady state and pre–steady state behavior of the NaP_i-2 isoform over a wide membrane potential and substrate concentration range. We show that this mammalian isoform functions in a kinetically similar way to the flounder isoform (NaP_i-5) recently described by Forster et al. (1997*a*), but with significant differences in the detailed kinetics. Moreover, we have identified and characterized a Na^+-slippage component in type II Na^+/P_i cotransport.

MATERIALS AND METHODS

Oocytes

Stage V-VI oocytes from the clawed frog *Xenopus laevis* were prepared according to standard procedures and injected with 10 ng/oocyte of cRNA encoding for the NaP_i-2 protein (Werner et al., 1990) 24–48 h after defolliculation. Cells were incubated at 16–18°C in modified Barth's solution (see below) and tested for expression 2–5 d after injection. Only cells having a resting membrane potential below -20 mV and a steady state leakage current <100 nA at -50 mV were used.

Electrophysiology and Data Acquisition

Oocytes were placed in a small recess in a plexiglas superfusion chamber (0.2 ml vol) and continuously superfused (5 ml/min) with ND96 control solution (see below). Computer controlled valves allowed fast and reproducible solution changes. All superfusates were cooled to 20–22°C before entering the chamber. Dose-response protocols were run with increasing concentration of the test substrate and the application time for P_i never exceeded 20 s to avoid possible loading of the cell. Long-term stability of the preparation was monitored using a chart recorder and each new test solution application was made only after the holding current had returned to the previous control value, with the test application always preceded by recording the response to the control solution. Oocytes were voltage clamped using a custom-built two-electrode voltage clamp with active series resistance compensation to improve the clamping speed. Furthermore, for the steady state recordings using the staircase protocol, an electronic transient subtraction stage was used to increase the ADC dynamic range to avoid overloading the data acquisition system. Cells were normally clamped at a holding potential of -50 mV to reduce possible contamination from Ca^{2+}-activated Cl^- currents at depolarized potentials. Current recordings were filtered using an eight-pole Bessel filter (902; Frequency Devices, Haverhill, MA) at a cut-off frequency less than twice the sampling frequency used. Data acquisition, voltage command generation, and solution valve control were done using laboratory built PC-compatible hardware and programmed using DATAC software (Bertrand and Bader, 1986).

Solutions and Chemicals

All reagents were obtained from Sigma Chemical Co. (St. Louis, MO) or Fluka (Buchs, Switzerland). Solutions were prepared as follows (mM/liter). (*a*) Oocyte incubation (modified Barth's solution): 88 NaCl, 1 KCl, 0.41 $CaCl_2$, 0.82 $MgSO_4$, 2.5 $NaHCO_3$, 2 $Ca(NO_3)$, 7.5 Tris, pH 7.6, supplemented with antibiotics (10 mg/liter penicillin, streptomycin). (*b*) Control superfusate (ND96): 96 NaCl, 2 KCl, 1.8 $CaCl_2$, 1 $MgCl_2$, 5 HEPES, titrated to pH 7.4 with NaOH. Isomolar $BaCl_2$ was routinely substituted for $CaCl_2$ to reduce contamination from endogenous Ca^{2+}-activated Cl^- currents that were observed for $V > -10$ mV and allow a greater range of P_i concentrations, except for experiments involving phosphonoformic acid (PFA), which otherwise complexes with Ba^{2+}. For Na^+-substitution experiments, *N*-methyl-D-glucamine replaced Na^+ at the appropriate concentration to maintain isoosmolar external solutions. Solutions were titrated with HCl or KOH to pH 7.4. (*c*) Test superfusate: inorganic phosphate such as $Na_2HPO_4.6H_20$, was added to the solutions in *b,* and pH was adjusted to 7.4. For the Na^+-substitution experiments, a KH_2PO_4/K_2HPO_4 buffer (pH 7.4) was used to minimize changes in Na^+ concentration. (*d*) PFA experiments: to take account of PFA being a trisodium salt, Na^+ was added in the appropriate concentration to the control solutions to give equal final Na^+ concentrations.

Data Analysis and Curve Fitting

Preliminary data analysis was performed using macro routines written in the DATAC language (Bertrand and Bader, 1986). Nonlinear regression analysis was performed using Inplot v. 4.0 or Prism v. 2.0 software (Graphpad Inc., San Diego, CA). All data are shown as mean ± SEM (n), where n is the number of oocytes for a particular protocol. Experimental protocols were repeated at least twice on different batches of oocytes from different frogs. Exponential curve fitting was performed using a Chebychev transform routine written in C.

Dose-response curves. Responses with respect to a variable substrate S, were quantified as peak P_i-induced current and a form of the Hill equation was fit to the dose response:

$$I_p = I_{pmax}[S]^n / \{[S]^n + (K_m^s)^n\}, \quad (1)$$

where $[S]$ is the substrate concentration, I_{pmax} the extrapolated maximum current, K_m^s the concentration of substrate S that gives a half maximum response or apparent affinity constant, and n the Hill coefficient.

Two-state Eyring-Boltzmann model for transmembrane charge movements. For a two-state system in which N charged entities, each having an apparent valency z, can translocate independently between two states within the transmembrane field, the macroscopic steady state charge distribution as a function of transmembrane voltage V, is given by:

$$Q = Q_{hyp} + Q_{max} / \{1 + \exp[-ze(V - V_{0.5}) / (kT)]\}, \quad (2)$$

where $Q_{max} = Nze$, the maximum charge translocated, Q_{hyp}, which depends on the holding potential, is the charge translocated at the hyperpolarizing limit, $V_{0.5}$ is the voltage at which the charge is distributed equally between the two states, e the electronic charge, k Boltzmann's constant, and T the absolute temperature.

Simulations. To simulate pre–steady state and steady state currents, the differential equations describing the state transitions were solved for the state occupancies by using matrix methods to find the eigenvalues and eigenvectors (e.g., Press et al., 1992). For any transition between states i and j involving an apparent charge movement ze, the forward and backward rate constants were expressed as $k_{ij} = K_{ij}\exp(-ze\delta V/kT)$ and $k_{ji} = K_{ji}\exp[ze(1 - \delta)V/kT]$, respectively, where K_{ij} and K_{ji} are the corresponding forward and backward rate constants, respectively, at $V = 0$ and δ is an asymmetry factor ($0 \leq \delta \leq 1$) that defines the relative position of the energy barrier within the transmembrane electric field (e.g., Adrian, 1978). For transitions involving substrate binding, the rate constant was scaled by the factor S^n, where S is the substrate concentration and n the number of ions involved in the binding reaction. Simulation routines were written in C and adapted from those given in Press et al. (1992). For simulations, the temperature was assumed to be 20°C.

RESULTS

Voltage Dependence of P_i Dose Response in the Steady State

Fig. 1 *A* shows the typical phosphate-induced current at two holding potentials (V_h) recorded from an oocyte expressing NaP_i-2 when the control superfusate was rapidly switched to a test solution containing 1.0 mM P_i. The dependence on V_h of the maximum steady state response confirmed that NaP_i-2 exhibited electrogenic behavior. Such currents were not observed when the same protocol was applied to water or noninjected oocytes (data not shown), as reported previously (Busch et al., 1994). With fast superfusion of the oocyte, the P_i-induced response gave a rapid initial phase, the rise time of which was limited by the recording bandwidth. This was followed by a slower relaxation phase before finally reaching a steady state level after ~10–15 s. Washout of P_i was also accompanied by a similar biphasic return to the baseline. At all potentials tested, the magnitude of the fast phase was proportional to V_h. We attributed the slower phase to the electrogenic response of regions of the oocyte membrane that did not experience an initial rapid exchange of superfusate due to unstirred layer effects. These oocyte-dependent response kinetics were not investigated further in this study. Once the maximum was reached, I_p usually remained constant for intervals exceeding 20 s.

To obtain the steady state current–voltage (I-V) relationship, it was convenient to apply a voltage staircase in the range −140 to +40 mV after the current at V_h had stabilized. The duration of each step (50 ms) was chosen so that a steady state was reached before the next voltage transition. This was also confirmed by checking that I_p at different holding potentials was the same as the step current corresponding to the same potential (data not shown). Some preliminary experiments were also performed using a continuous ramp of 1-s duration and the results were indistinguishable from the staircase (Forster et al., 1996).

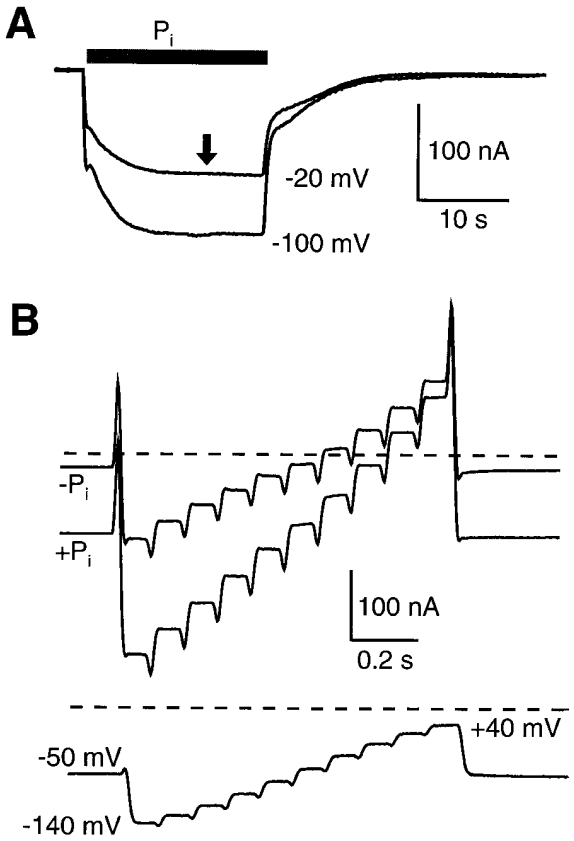

FIGURE 1. Voltage-dependent P_i-induced currents in an oocyte expressing the NaP_i-2 cotransporter. (*A*) Inward currents measured in response to the application of 1.0 mM P_i during the period indicated by the horizontal bar, at two holding potentials. Baseline current offsets have been suppressed to show P_i-induced current only. Arrow indicates time at which the staircase protocol (shown in *B*) is applied. Note that a similar fast change in current accompanies both application and washout of P_i. The ratio of initial fast component amplitude to the steady state current was the same for both potentials and depended on the superfusion conditions. The slower component possibly reflects the rate of P_i diffusion through the unstirred layer of oocyte that is not directly exposed to the superfusate. The cell was bathed in standard ND96 solution (see MATERIALS AND METHODS). (*B*) Response of another oocyte expressing NaP_i-2 to voltage staircase protocol applied ~17 s after application of P_i (*A, arrow*). Each step corresponds to a −20-mV membrane potential change. Same superfusion conditions as in *A*. (*top traces*) Response to voltage staircase, from −140 to +40 mV, superimposed on −50-mV holding potential (V_h) in the absence ($-P_i$) and presence ($+P_i$) of 1 mM P_i. Note that the steady state current immediately before and after the staircase is the same in each case. The current spike at each voltage transition results from incomplete cancellation of the endogenous capacitive transient and pre–steady state relaxations using the capacitive transient simulator (see MATERIALS AND METHODS). (*bottom*) P_i-induced current obtained by subtraction of the two traces. Dashed line indicates zero holding current level.

Fig. 1 *B* shows the typical response to a voltage staircase, starting after I_p had stabilized, in the absence and presence of 1.0 mM P_i in the superfusate. The small transient at each transition indicates incomplete suppression of the endogenous oocyte capacitive transient (see MATERIALS AND METHODS) due to P_i suppression of the pre–steady state response. The I-V relationship for the P_i-dependent current was obtained directly from the difference between these records, as shown in the bottom trace. In the physiological range of potentials ($-60 < V < -20$ mV), the I-V relation was linear, whereas at strong depolarizing and hyperpolarizing potentials, it deviated from linearity. This behavior suggested the presence of rate-limiting, voltage-independent steps in the transport mechanism.

To characterize further the NaP_i-2 voltage dependency in the steady state, we applied the staircase protocol with different P_i and fit Eq. 1 to the dose-response data at each potential. The resulting family of I-V data for a typical cell at 96 mM Na^+ is shown in Fig. 2 *A* for six P_i values in the range 0.006–1 mM. Typically, no current reversal was observed, although with some oocytes at low P_i (<0.01 mM) the P_i-induced current did show reversal at potentials <0 mV. This behavior was not reproducible, but appeared to be dependent on the oocyte batch/donor frog. These apparent outward cur-

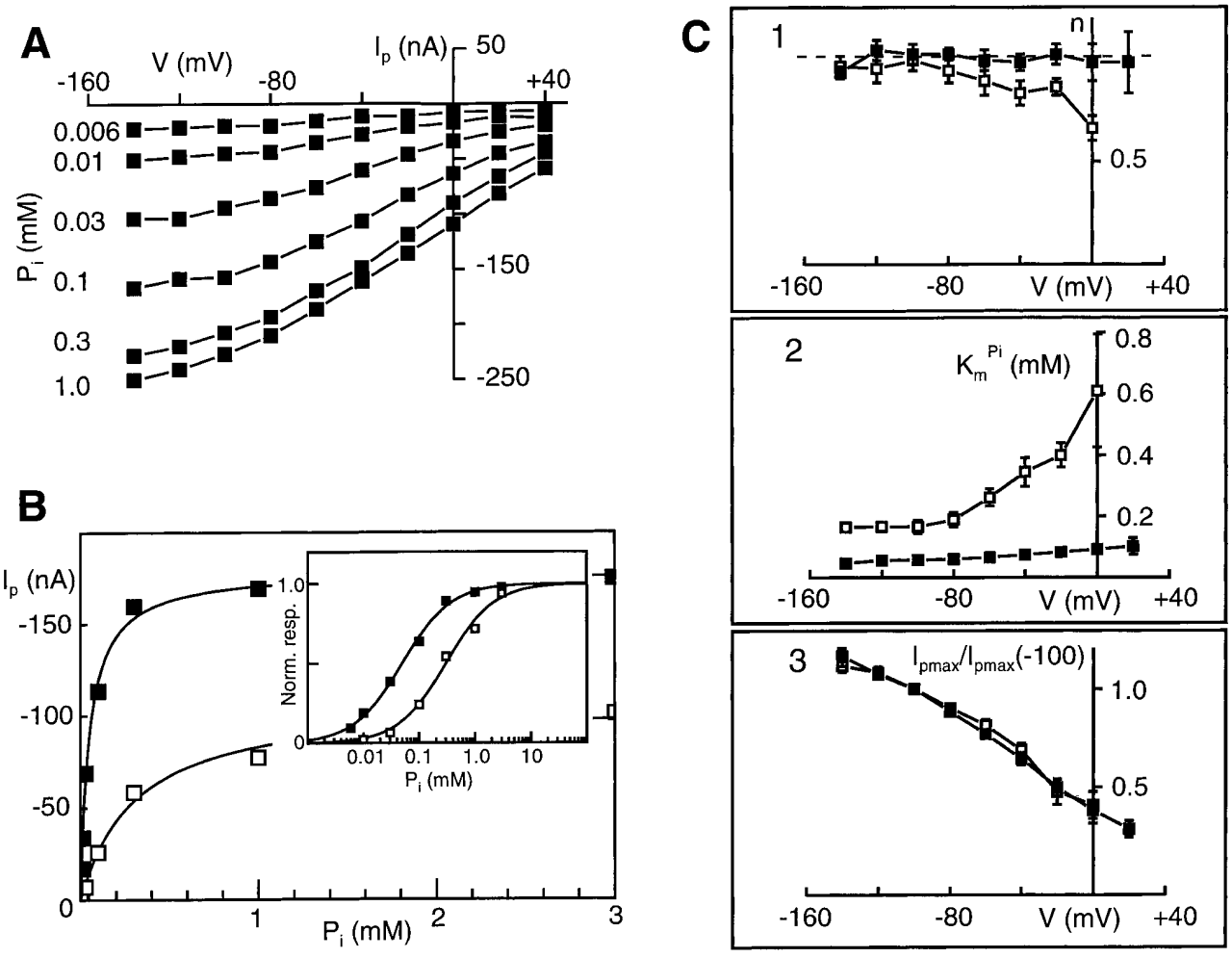

FIGURE 2. Steady state voltage dependency of Na^+/P_i transport as a function of P_i. (*A*) Typical set of I-V curves obtained using staircase protocol (Fig. 1 *B*) applied to one cell with 96 mM Na^+ and P_i in the range 0.006–1.0 mM as indicated. Data points are joined for visualization only. Note the absence of zero crossing for $V > 0$. (*B*) Representative dose-response curves at $V_h = -50$ mV for two concentrations of Na^+: 96 (■), 50 (□) mM and the same cell with P_i as the variable substrate. Eq. 1 was fit to the raw data with the following parameters: (96 mM Na^+) $K_m^{Pi} = 0.054$ mM, $n = 0.8$, $I_{pmax} = 74$ nA; and (50 mM Na^+) $K_m^{Pi} = 0.27$ mM, $n = 0.9$, $I_{pmax} = 50$ nA. Inset shows the same data normalized to maximum predicted response and plotted semi-logarithmically to indicate clearly the shift in K_m^{Pi}. (*C*) Summary of voltage dependency of fitted parameters comparing data for two concentrations of Na^+: 96 (■) and 50 (□) mM pooled from different cells. Data are shown as mean ± SEM ($N = 4$). Only SEMs exceeding symbol size are shown. Data points are joined for visualization only. (*C, 1*) n = Hill coefficient, (*dashed line*) $n = 1$; (*C, 2*) K_m^{Pi} = apparent affinity constant; (*C, 3*) $I_{pmax}/I_{pmax(-100)}$ = maximum induced current normalized to the value at −100 mV.

rents at −140 mV typically did not exceed 5% of the peak induced current at 1 mM P_i and most likely reflect the instability of the preparation as they would become more apparent when subtracting two quantities of similar magnitude. We derived the steady state P_i dose response with respect to the magnitude of I_p from these data at the same V_h (−50 mV) for two Na^+ concentrations (96 and 50 mM) and the same oocyte (Fig. 2 *B*). The form of the dose-response relationships resembled a rectangular hyperbola with clear evidence of saturation at high P_i. Fitting Eq. 1 to these data indicated that, for a reduction in Na^+ from 96 to 50 mM, the predicted maximum induced current (I_{pmax}) was significantly reduced by 38 ± 5% (N = 5) at 50 mM Na^+, when comparing the responses from the same five oocytes. Moreover, the fit indicated that the half-maximum concentration for P_i (K_m^{Pi}) increased from 0.057 ± 0.006 mM at 96 mM Na^+ to 0.35 ± 0.03 mM at 50 mM Na^+ for the same five oocytes. The shift in K_m^{Pi} is seen more clearly by normalizing the data to I_{pmax} and plotting on a semilogarithmic scale (see Fig. 2 *B, inset*). Finally, in agreement with previous results (Busch et al., 1995; Hartmann et al., 1995), the estimated Hill coefficient (n) was close to unity for both concentrations (at 96 mM Na^+, n = 0.96 ± 0.05 and at 50 mM Na^+, n = 0.92 ± 0.06).

From the Hill equation fits, we determined the potential dependence of the estimates for n, K_m^{Pi}, and I_{pmax}, pooled from representative cells from different donor frogs (Fig. 2 *C*). Reliable estimates of current were restricted to voltages <0 mV for both Na^+ concentrations. The Hill coefficient was close to unity for each Na^+ concentration and showed little dependence on V (over the range −140 ≤ V ≤ 0 mV, at 96 mM Na^+, n =

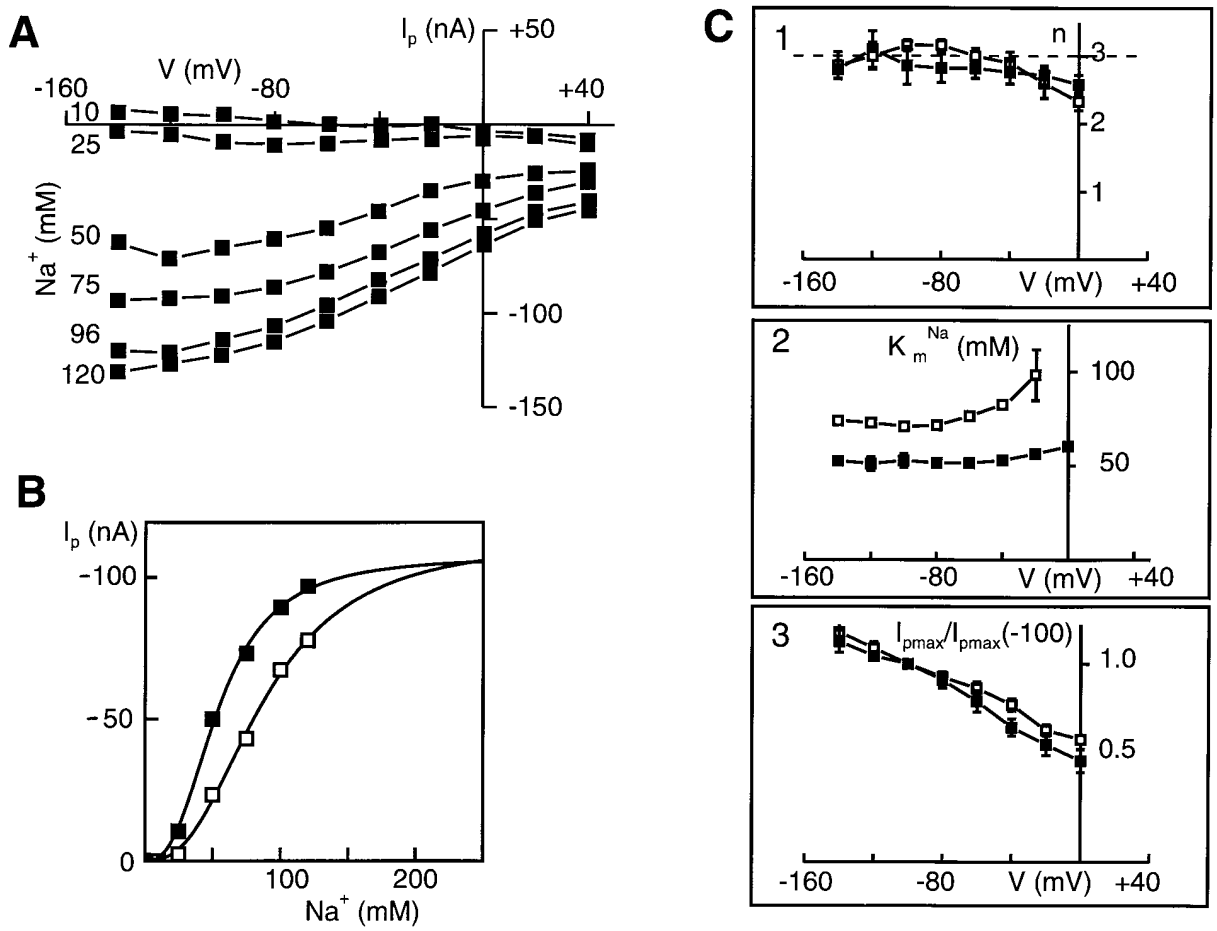

FIGURE 3. Steady state voltage dependency of Na^+/P_i transport as a function of Na^+ concentration. (*A*) Typical family of I-V curves obtained from one cell with 1 mM P_i and six Na^+ concentrations as indicated (millimolar). Data points are joined for visualization only. (*B*) Typical dose-response data for the same cell at two P_i concentrations: 1.0 (■) and 0.1 (□) mM with Na^+ as the variable substrate and V_h = −50 mV. Eq. 1 was fit to the data points. For this cell, the fit parameters were: (1 mM P_i) K_m^{Na} = 50.1 mM, n = 2.6, I_{pmax} = 109 mM; and (0.1 mM P_i) K_m^{Na} = 89 mM, n = 2.6, I_{pmax} = 114 mM. (*C*) Summary of voltage dependence of fitted parameters comparing data for two concentrations of P_i: 1 (■) and 0.1 (□) mM. Data are shown as mean ± SEM. Only SEMs exceeding symbol size are shown. Data points are joined for visualization only. (*C, 1*) n = Hill coefficient, (*dashed line*) n = 3; (*C, 2*) K_m^{Na} = apparent affinity constant; (*C, 3*) $I_{pmax}/I_{pmax(-100)}$ = maximum induced current normalized to the value at −100 mV.

1.0 ± 0.01 and at 50 mM Na^+, $n = 0.87 \pm 0.03$) (Fig. 2 *C, top*). At 50 mM Na^+, n was significantly smaller than at 96 mM Na^+, particularly at higher V. At 96 mM Na^+, K_m^{Pi} (Fig. 2 *C, middle*) was weakly voltage dependent and increased by ~60% over the voltage range from V = −140 to V = +20 mV. At 50 mM Na^+, the increase in K_m^{Pi} was fourfold over the same range of V, with a significant change occurring in the physiological range (−70 < V < −20 mV). Finally, the voltage dependence of I_{pmax} for the two Na^+ concentrations superimposed when normalized to the current at −100 mV (Fig. 2 *C, bottom*), indicating that the voltage dependence of I_{pmax} was the same for the two Na^+ concentrations tested at saturating P_i.

Voltage Dependence of Na^+ Dose Response in the Steady State

Next we studied the voltage dependency of NaP_i-2 transport as a function of external Na^+ with fixed P_i, using the same methods as above. Fig. 3 *A* shows a typical set of I-V curves for the same oocyte with 1 mM P_i and six Na^+ concentrations. For $Na^+ > 25$ mM, the I-V curves showed no current reversal up to +40 mV. For this particular cell at 10 mM Na^+, the P_i-induced current reversed at −40 mV. As noted above, the variability of this apparent reversal reflects the precision of the subtraction/recording procedure and should not be taken as a true indication of current reversal. We generated I-V curves in response to the staircase protocol at two P_i concentrations: 1 mM (close to saturating P_i) and 0.1 mM (close to K_m^{Pi}). We were unable to make reliable determinations of the I-V relations at $P_i < 0.1$ mM and $Na^+ < 50$ mM because of the small magnitude of the induced currents (typically < 10 nA), the estimation of which was sensitive to any drift in the endogenous holding current during the course of the experiment.

Fig. 3 *B* shows the typical steady state dose response for the same cell with the two P_i concentrations at −50 mV holding potential. Plotted on a linear abscissa, the dose–response relationship was sigmoidal with an inflection at low Na^+, typical for cooperative substrate binding and consistent with our previous results (Busch et al., 1994, 1995). Fitting Eq. 1 to these data was less reliable than for the P_i dose dependency determination because of the absence of clear saturation at the maximum Na^+ concentration possible, particularly at 0.1 mM P_i. We attempted to superfuse the oocytes with $Na^+ > 120$ mM for short periods, but the hyperosmotic conditions resulted in significant holding current instability. Despite this limitation, the results of fitting Eq. 1 to these data suggested that the predicted I_{pmax} was independent of P_i (at $V_h = -50$ mV, the ratio I_{pmax}[1 mM P_i]/I_{pmax}[0.1 mM P_i] = 1.08 ± 0.03, $N = 5$). Furthermore, at $V_h = -50$ mV, the estimated Hill coefficient was close to 3 in both cases (at 0.1 mM P_i, $n = 2.9 \pm 0.1$ and at 1 mM P_i, $n = 2.9 \pm 0.2$, $N = 5$), whereas the apparent affinity constant for Na^+ (K_m^{Na}) was clearly P_i dependent. For the same five cells at $V_h = -50$ mV with 1 mM P_i, $K_m^{Na} = 52.0 \pm 2.2$ mM and with 0.1 mM P_i, $K_m^{Na} = 81.8 \pm 2.3$ mM.

Fig. 3 *C* shows the voltage dependence of the three fit parameters (K_m^{Na}, n, and I_{pmax}) for the two P_i concentrations, pooled from oocytes from different donor frogs. For both P_i, n (Fig. 3 *C, top*) remained approximately voltage independent over the physiological range of potentials (at 1.0 mM P_i, $n = 2.81 \pm 0.04$ and at 0.1 mM P_i, $n = 2.89 \pm 0.08$). Furthermore, at 0.1 mM P_i, K_m^{Na} (Fig. 3 *C, middle*) increased monotonically with depolarizing membrane potential, whereas at 1 mM P_i the voltage dependence was less marked and the normalized voltage dependence of I_{pmax} for the 10-fold reduction in P_i showed a small but consistent deviation as V approached 0 mV (Fig. 3 *C, bottom*). This suggested that the voltage sensitivity of the rate limiting step(s) was reduced at the lower P_i for saturating Na^+.

Suppression of I_p by Phosphonoformic Acid Reveals a Na^+-dependent Current in the Absence of External P_i

We tested for the presence of slippage in the type II Na^+/P_i system using PFA, a competitive inhibitor of Na^+/P_i cotransport (Busch et al., 1995; Kempson, 1988). Fig. 4 *A* shows measurements of the holding current (I_h) at $V_h = -50$ mV made at 5-s intervals for a typical oocyte expressing NaP_i-2 and a noninjected oocyte from the same batch, in response to the application of substrate combinations indicated. For NaP_i-2, in 105 mM Na^+, 0.3 mM P_i induced an increase in I_h of 89 nA, whereas in the presence of 3 mM PFA, I_h increased by only ~9 nA, which confirmed the inhibitory effect of PFA. In contrast, the noninjected oocyte showed a 2-nA change in the presence of 0.3 mM P_i, which might be attributable to an endogenous Na^+/P_i cotransporter, and a similar change also occurred in the presence of PFA. For both cells, in the absence of P_i, switching Na^+ between 9 and 105 mM led to a concomitant change in I_h. This would be expected if a component of I_h were due to a Na^+ conductance, although in the case of NaP_i-2, the change was fivefold larger. Moreover, for cells expressing NaP_i-2, 3 mM PFA suppressed I_h at 105 mM Na^+ by ~50% and induced the same relative decrease at 9 mM Na^+, whereas no measurable shift in I_h occurred for the noninjected cell. This behavior would be consistent with the PFA-sensitive component (I_{PFA}) being due to a Na^+ conductance. If this were the case, we would predict a shift in the reversal potential (E_r) for I_{PFA} in response to a change in external Na^+. Fig. 4 *B* shows a typical I-V relation for I_{PFA} for two external Na^+ (109 and 59 mM), obtained by subtracting the response to a staircase voltage protocol in the presence of 3 mM PFA from the response in the absence of PFA.

The expected shift towards a more negative E_r was found and, moreover, this behaved in a Nernstian manner for the three Na^+ concentrations tested, giving a slope of 64.4 ± 1.7 mV. We were unable to determine E_r reliably for $Na^+ < 50$ mM due to the small magnitude I_{PFA}. The Na^+ dependence of this component was characterized further by determining the dose dependency at −50 mV, as shown in Fig. 4 *C* for a typical cell expressing NaP_i-2. The relation was nonlinear, indicating saturation of this pathway and, when Eq. 1 was fit to these data, we obtained a K_m = 128 mM and a Hill coefficient of 0.92 (n = 1). Finally, the magnitude of I_{PFA} correlated linearly with the P_i-induced current for a number of oocytes from different batches and with different levels of expression, indicating that I_{PFA} was ~12% of the P_i-induced current at 1 mM P_i. (Fig. 4 *D*).

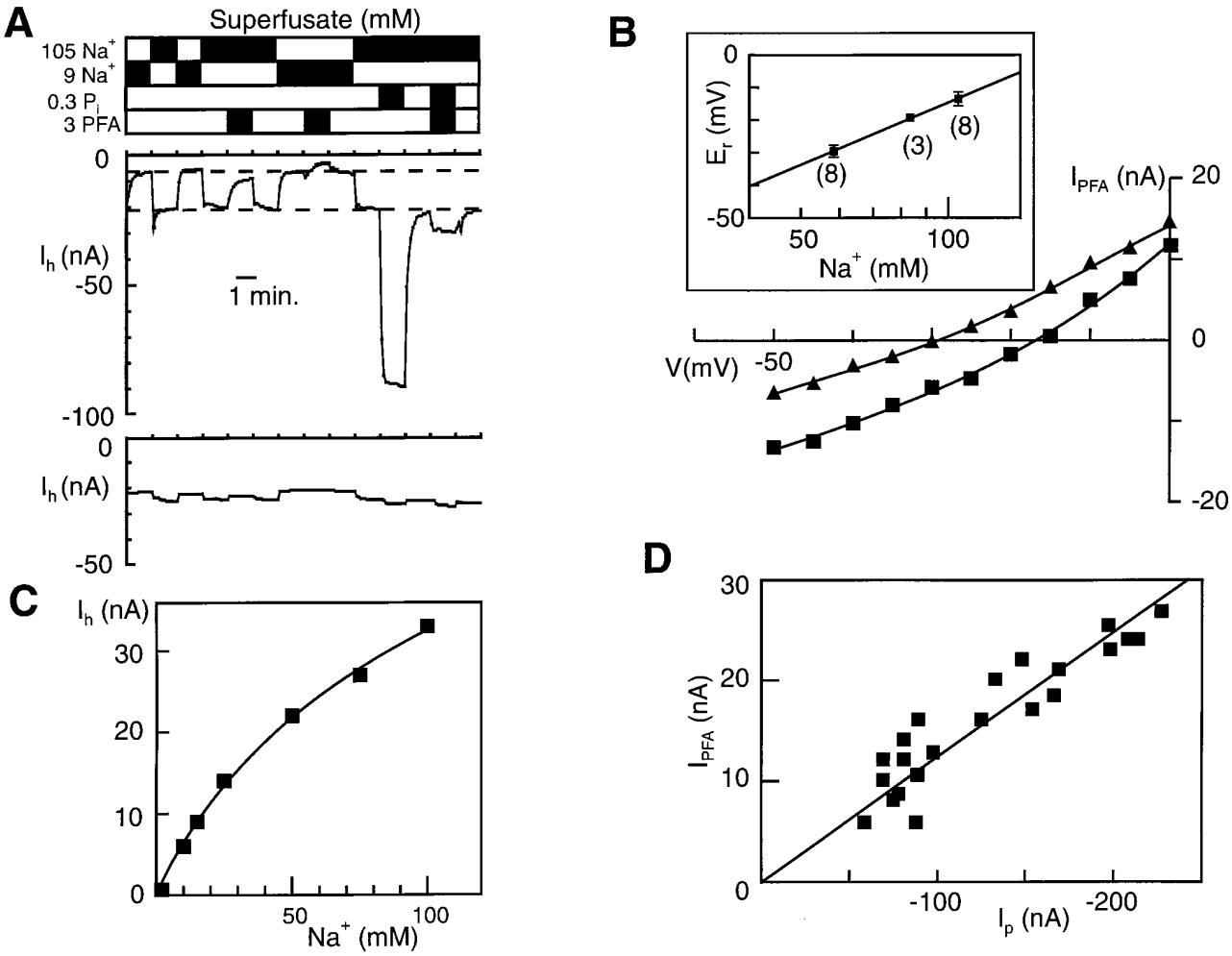

FIGURE 4. Characterization of P_i-independent current component using phosphonoformic acid. (*A*) Oocyte holding current (I_h) at V_h = −50 mV for continuous superfusion with the indicated solutions for a NaP_i-2-expressing oocyte (*top*) and noninjected oocyte (*bottom*) from the same batch of oocytes and recorded during the same experimental session. I_h was sampled at 5-s intervals and the sample points have been joined by straight lines for clarity. Each superfusate combination was applied for 1 min to allow a stable baseline to be reached. Top and bottom dashed lines, superimposed on NaP_i-2 data, indicate I_h at 9 and 105 mM Na^+, respectively. (*B*) Typical I-V relations for the PFA-sensitive component at two concentrations of Na^+: 109 (■) and 59 (▲) mM. A staircase voltage protocol with 5-mV, 100-ms-long steps was applied to the oocyte. Points represent the difference between the steady state current at the end of each step under control conditions and the response in the presence of 3 mM PFA. As PFA is a trisodium salt, the control solution Na^+ concentration in each case was adjusted to ensure that the Na^+ gradient remained the same. Continuous lines are polynomial fits to the data, used to determine the reversal potential (E_r). Inset shows E_r plotted as a function of Na^+ concentration. Note that Na^+ concentration is plotted on a $\log_{10}$ scale. Number of cells is indicated for each Na^+ tested. Straight line is a linear regression giving a slope 64.4 ± 1.7 mV. (*C*) Dose dependency with respect to Na^+ for I_h in the absence of P_i at V_h = −50 mV. Data shown for a typical cell expressing NaP_i-2. Each point represents the induced change in steady state current, relative to 0 mM Na^+. Continuous curve is the fit using Eq. 1, giving K_m = 128 mM, I_{hmax} = 74 nA, and n = 0.92. (*D*) The PFA-sensitive current correlates with the P_i-induced current. Data shown for 22 cells from several donor frogs displaying different levels of expression of NaP_i-2. For each cell, the P_i-induced current (I_p) at 1 mM P_i was determined together with the PFA-sensitive component (I_{PFA}) for 3 mM PFA at V_h = −50 mV. The straight line is a linear regression line forced through the origin with a slope: 0.126 ± 0.004.

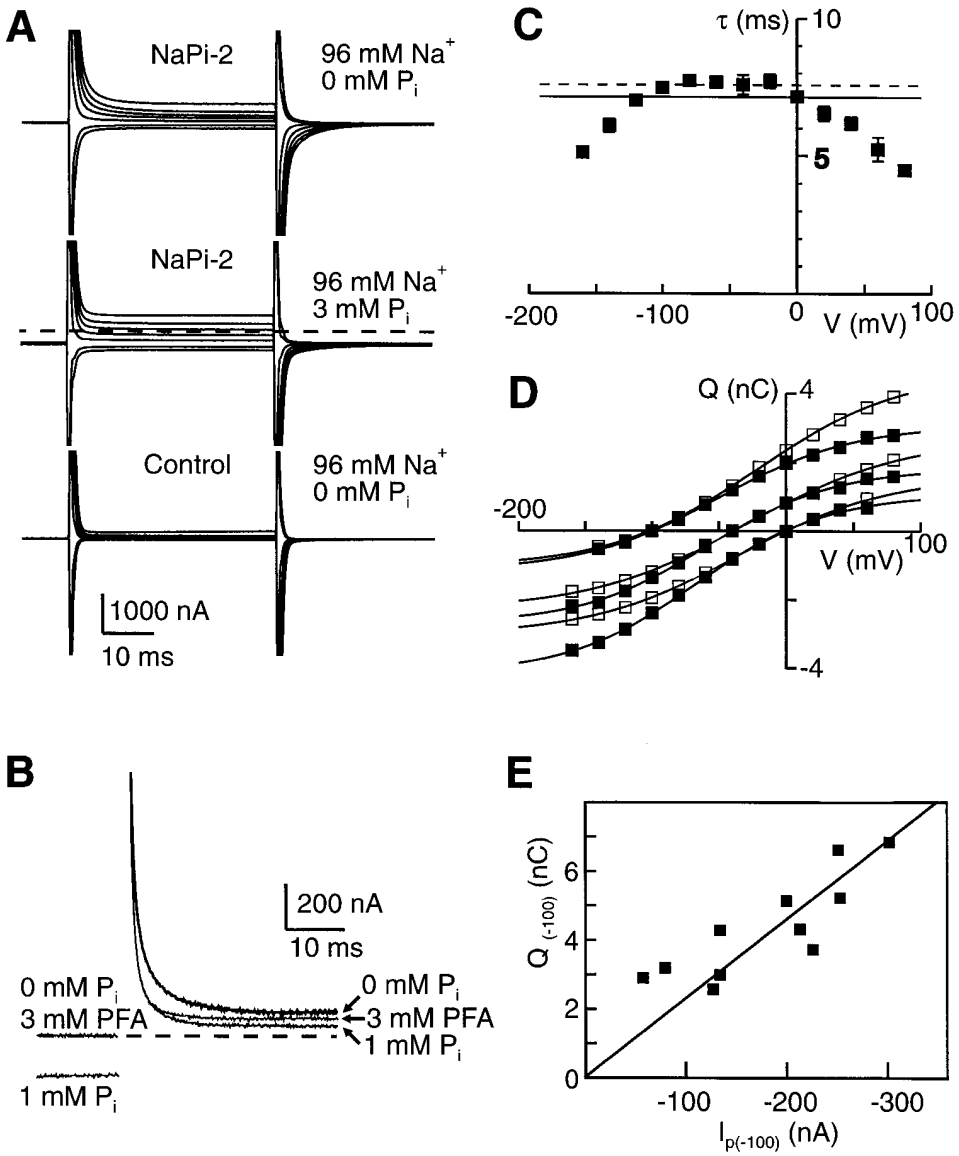

FIGURE 5. Pre–steady state relaxations induced by voltage steps applied to oocytes expressing NaP_i-2. (*A*) Family of current records in response to voltage steps from $V_h = -100$ to -140, -120, -80, -40, 0, $+40$, and $+80$ mV, and returning to V_h after 40 ms. (*top*) Superfusion with 96 mM Na^+, 0 mM P_i. The endogenous capacitive charging transients of the oocyte have been clipped due to the high voltage clamp gain used. (*middle*) Superfusion with 96 mM Na^+, 3 mM P_i. Dashed line, corresponding to the holding current level at -100 mV in the absence of P_i, is superimposed to indicate the change in steady state current induced by P_i (at -100 mV, $I_p \approx 250$ nA). (*bottom*) Superfusion with 96 mM Na^+, 0 mM P_i for a noninjected oocyte from the same batch. Each record is the average of eight successive raw sweeps. Filtering at 3 kHz, sampling 50 μs/point. (*B*) Effect of PFA pre–steady state currents. Records in response to a voltage step from -100 to 0 mV for superfusion in the presence of 0.3 mM P_i or 3 mM PFA compared with the response for 96 mM Na^+ alone, as indicated. Dashed line indicates baseline for control condition. Each record is the average of eight successive raw sweeps and has been blanked for 2 ms during the capacitive charging transient. Filtering at 3 kHz, sampling 50 μs/point. (*C*) Voltage dependency of the main time constant (τ) obtained from biexponential fit to records such as in *A* for holding potentials (V_h) -100, -40, and 0 mV for the same cell. Filled symbols are mean ± SEM of the ON transition τs at the three V_h. The straight lines represent the mean of the OFF relaxation τs over the whole voltage range: (*dotted line*) $V_h = -100$ mV, (*dashed line*) $V_h = 0$ mV. The mean OFF τs are: 7.5 ± 0.06 ms ($V_h = -100$ mV); 7.6 ± 0.05 ms ($V_h = -40$ mV), and 7.13 ± 0.14 ms ($V_h = 0$ mV). (*D*) Voltage dependency of charge movement (Q) associated with NaP_i-2-related component at different V_h for the same cell as in *B*. (■) ON, (□) OFF. Continuous lines are fits of the Boltzmann function (Eq. 2) to the data. See Table I for fit parameters. (*E*) Correlation between estimated charge available for translocation at -100 mV ($Q_{(-100)}$) and P_i-induced current at -100 mV ($I_{p(-100)}$) with 96 mM Na^+ and 1 mM P_i. Data points are from 11 cells from different oocyte batches. $Q_{(-100)}$ was obtained by fitting the Boltzmann function (Eq. 2) to the Q-V data and $I_{p(-100)}$ was obtained from steady state response of same cell under same recording conditions. Straight line is a linear regression line with slope 46 s^{-1} and forced to intercept the origin.

Voltage Steps Induce Pre–Steady State Relaxations Typical of Na^+-coupled Cotransporters

Voltage steps induced pre–steady state relaxations in oocytes expressing NaP_i-2 (Fig. 5 *A*). The speed of relaxation to the steady state after a voltage step depended on the presence of P_i in the superfusate. In the absence of P_i (Fig. 5 *A*, *top*), pre–steady state relaxations, superimposed upon the normal capacitive charging transient, were observed when the membrane potential of NaP_i-2-expressing oocytes was stepped from a holding potential, $V_h = -100$ mV. Relaxations were significantly suppressed when the cell was superfused with saturating P_i (3 mM) in the presence of 96 mM Na^+ (Fig. 5 *A*, *middle*) and were absent in noninjected oocytes from the same batch (*bottom*). Apart from the difference in the steady state current at the test potential, the

records for the noninjected cell and NaP_i-2 with 3 mM P_i appeared very similar.

To establish further that these relaxations were specifically related to the expression of NaP_i-2, we examined the effect of superfusing with the inhibitor PFA. Fig. 5 *B* compares the current induced by a voltage step from −100 to 0 mV for superfusion with 3 mM PFA and 1.0 mM P_i. PFA suppressed the pre–steady state relaxation when compared with the control condition, analogous to the suppression by 1.0 mM P_i alone.

Exponential curve fitting allowed separation of the intrinsic oocyte charging component from the relaxation related specifically to NaP_i-2. The fits were quantitated in terms of the time constant (τ) and charge transfer (Q) estimated from the product of τ and the amplitude of the NaP_i-2-specific component extrapolated to time of respective voltage step onset. Biexponential curve fitting consistently showed that the faster (intrinsic) τ varied little with voltage (typically 0.6 ± 0.1 ms for $-140 < V < +60$ mV) or with the direction of the voltage step (data not shown). Often, however, when tuning the voltage clamp for fastest response, we observed that the intrinsic capacitive transient displayed an additional tail component with a $\tau \approx 1$ ms (see Fig. 7 *B, inset*), which was also observed in control oocytes from the same batch. Superfusion of control oocytes with 20 μM ouabain did not alter this component, suggesting that it did not arise from intrinsic Na/K pump (Holmgren and Rakowski, 1994). To ensure that any such intrinsic components did not influence the fit accuracy, the P_i-suppressed relaxation was characterized by fitting a single exponential, starting ~5 ms after the step. Fig. 5 *C* shows the voltage dependence of the slower τ obtained from a typical oocyte for three holding potentials (V_h). The ON transition relaxation kinetics showed a bell-shaped relation expected for voltage-dependent charge movements, whereas those for the corresponding OFF transition were independent of the voltage reached before returning to the holding potential. Moreover, the OFF transition τ at each V_h coincided with the interpolated value for the ON transition at that test voltage.

Fig. 5 *D* shows the voltage dependence of the corresponding steady state charge transfer for the same oocyte. These data indicate that the charge transfer tended to saturate at strong depolarizations. This suggested that the detected relaxation behaved as expected for movement of a fixed number of translocatable charges within the transmembrane field. Furthermore, we consistently observed that charge balance for the corresponding ON and OFF transitions occurred only over the mid-range of test potentials: the magnitude of the Q_{ON} and Q_{OFF} deviated at extreme test potentials that could not be simply attributed to random error in the fit. The continuous lines in Fig. 5 *D* are fits using the Boltzmann equation (Eq. 2) to give parameters that facilitated comparison of the pre–steady state currents under different conditions. Although the lack of clear saturation at extreme potentials made fitting error prone, the fits at different V_h revealed several consistencies (Table I): the apparent valency was independent of V_h, and the mid-point voltage ($V_{0.5}$), equivalent to the potential at which half the available charge was translocated, varied little with V_h, as did the total charge transfer, Q_{max}.

Finally, at $V_h = -100$ mV, the charge available for translocation from −100 mV, predicted from the Q-V fit (equivalent to the Q-V asymptote for $V >> 0$ and $V_h = -100$ mV), correlated linearly with I_p at −100 mV for several oocytes having different apparent NaP_i-2 expression levels (Fig. 5 *E*). The slope was 46 s^{-1}, and this parameter was used to estimate the transporter turnover (see DISCUSSION).

Substrate Dependence of Pre–Steady State Relaxations

As both substrates carry charge and could influence directly or indirectly the observed charge movements, we characterized the substrate dependence of relaxation kinetics and steady state charge distribution to identify the origin of pre–steady state relaxations.

Dependence on Na^+ in the absence of P_i. Fig. 6 *A* shows representative records of pre–steady state relaxations for a cell expressing NaP_i-2 with external Na^+ varying from 96 to 0 mM in response to a voltage jump from −100 to 0 mV. For comparison purposes, the pre–steady state response for the same cell when superfused with 3 mM P_i and 96 Na^+ is also shown. These data indicate: (*a*) for both the ON and OFF transitions, a component of the total pre–steady state charge movement was contributed by the presence of Na^+ that appeared to diminish with decreasing Na^+; (*b*) in the absence of external Na^+, a NaP_i-2-related charge movement was still present; and (*c*) under saturating P_i, the residual charge was further suppressed. This residual component was most likely not an oocyte-intrinsic charge movement since it was not observed in recordings from noninjected cells from the same oocyte batch (data not shown).

TABLE I

The Effect of Holding Potential on the Steady State Charge Distribution

V_h (mV)	−100		−40		0	
Transition	ON	OFF	ON	OFF	ON	OFF
z	0.45	0.50	0.43	0.53	0.45	0.45
$V_{0.5}$ (mV)	−22	−50.3	−28.7	−58.4	−34.3	−62.1
Q_{max} (nC)	5.70	4.25	5.00	4.53	4.63	5.62

Parameters obtained from a fit of the Boltzmann function (Eq. 2) to the Q-V data for the ON and OFF transitions ($n = 1$).

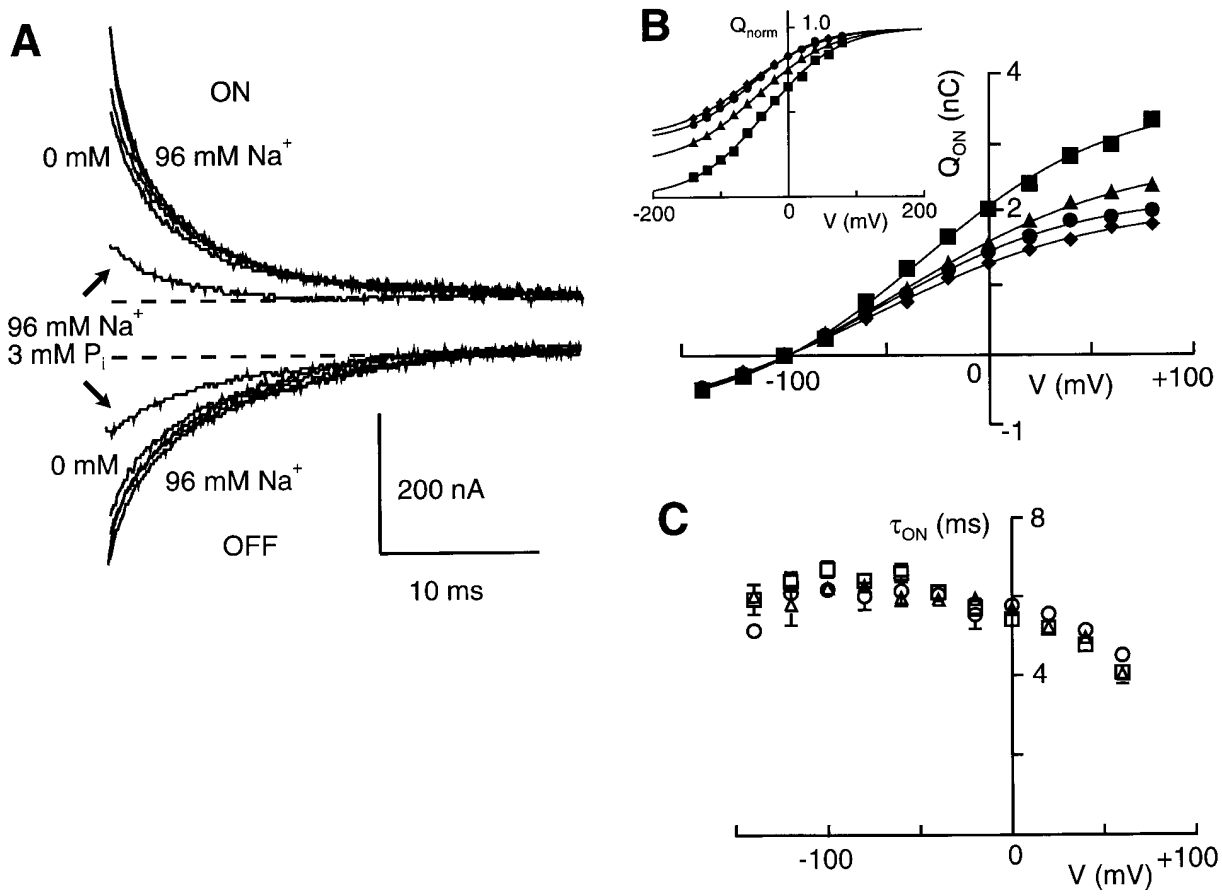

FIGURE 6. The effect of changing external Na^+ on pre–steady state relaxations. (*A*) Typical response to a voltage step from −100 to 0 mV for a cell expressing NaP_i-2 (I_p = −120 nA at −50 mV, 3 mM P_i). The cell was superfused with 96, 50, 25, and 0 mM Na^+ and sufficient time was allowed between changing superfusate to establish a steady holding current before making pre–steady state recordings. The pre–steady state response to superfusion with 96 mM Na^+ and 3 mM P_i is also shown. For superfusion with 0 mM Na^+ and 3 mM P_i, the response was the same as for 0 mM Na^+ alone (data not shown). All traces were blanked for the first 2 ms after the step and adjusted to give the same steady state baseline. (*B*) Steady state charge distribution under varying Na^+. The Q-V data (ON transition) for a typical cell with superfusion with 96 (■), 50 (▲), 25 (●), and 10 (◆) mM Na^+. Continuous lines were obtained by fitting the Boltzmann function (Eq. 2) to the data. Inset shows the same data normalized to the predicted maximum charge and offset to superimpose at the depolarizing limit to indicate the shift in $V_{0.5}$. (*C*) τ-V data pooled (n = 4) showing main ON relaxation time constant determined for superfusion with 96 (□), 50 (△), and 25 (○) mM Na^+.

The voltage dependence of the NaP_i-2-related charge movement and relaxation kinetics are summarized in Fig. 6, *B* and *C*, respectively. The Q-V data from a representative cell (Fig. 6 *B*) indicate that for a given voltage step from V_h = −100 mV a decrease in translocated charge occurred with reduced Na^+. If these data are normalized to the predicted Q_{max} at 96 mM Na^+ and offset to superimpose at the depolarizing limit, $V_{0.5}$ shifted negatively with decreasing Na^+ (see Fig. 6 *B, inset*). Moreover, the τ-V data, pooled from four representative cells (Fig. 6 *C*) showed the same general form of voltage dependence, but with an indication that the maximum τ was slightly reduced at the lower Na^+. Curve fitting was less reliable at low Na^+ because of the poorer signal-to-noise ratio and as a result we did not attempt fitting at 10 or 0 mM Na^+. The pooled results of the Boltzmann fit to the ON charge movement are summarized in Table II: the apparent valency, z, varied little with Na^+, whereas there was relative mean shift of −25 mV in $V_{0.5}$ with a fourfold reduction in Na^+, and the predicted Q_{max} decreased by only ∼20% over the same range.

Dependence on P_i with 96 mM Na^+. Pre–steady state relaxations induced by a voltage step from V_h = −100 to 0 mV, observed in the absence of P_i, were progressively suppressed with increasing P_i (Fig. 7 *A*). The voltage dependence of the NaP_i-2 relaxation was not affected by increasing P_i up to 0.1 mM with no consistent shift in $V_{0.5}$ and no change in the τ-V (data not shown). For $P_i \geq 0.1$ mM, the relaxations were too small to fit reliably over the entire voltage range. To characterize the effect of P_i further and facilitate quantification of the

TABLE II

The Effect of Changing External Na^+ on the Steady State Charge Distribution

Na^+ (mM)	96	50	25
z	0.48 ± 0.03	0.51 ± 0.03	0.46 ± 0.02
$\Delta V_{0.5}$ (mV)	0	−16.4 ± 2.6	−24.7 ± 2.5
Q_{max}/Q_{max} (96)	1.0	0.88 ± 0.02	0.78 ± 0.03

Fit parameters obtained from fitting the Boltzmann function (Eq. 2) to the Q-V data (mean ± SEM, $N = 4$). $\Delta V_{0.5}$ is the shift in $V_{0.5}$ relative to the value at 96 mM Na^+.

relaxations, we subtracted the corresponding relaxation under saturating conditions (3 mM P_i) from the record at the test P_i for test potentials in the range −100 to +80 mV (Fig. 7 *B*). The validity of this procedure was based on the assumption that a saturating concentration of P_i would fully suppress the relaxations (see Fig. 5 *A*). The resulting difference record should then have the oocyte endogenous charging transient eliminated and provide a measure of the amount of charge suppressed by the respective P_i superimposed on the steady state P_i-induced current. When we attempted to fit a single exponential to the P_i-dependent relaxations, this gave a significantly worse fit compared with a bi-exponential fit, although at large P_i, where most of the apparent translocatable charge was suppressed, the concomitantly poorer signal-to-noise ratio made such fitting more ambiguous. The fitting revealed a fast component (typical τ = 700–1,000 μs) with a weak voltage dependence and a slower component that corresponded to the main relaxation observed in the unmanipulated records. We were unable to detect any significant dependence on P_i for either component. The rapid speed of capacitive charging for this cell (see Fig. 6 *B, inset*) with a main τ = 191 μs, indicated that after 1 ms most of the membrane charging was complete and that the faster relaxation, revealed by the subtraction procedure, was most likely a true component of the total pre–steady state relaxation. To quantify the associated charge transfer, we integrated the total relaxation, commencing 1 ms after the voltage step. We also noted that the charge balance over the whole voltage range was consistently improved with the subtraction technique, resulting in <10% error in charge balance for $-140 \leq V \leq +60$ mV. The charge suppressed by P_i for four target potentials is shown in Fig. 7 *C*, and a competition curve (Eq. 1, with $n = -1$) was fit to the data points to give an apparent K_d^{Pi} as a

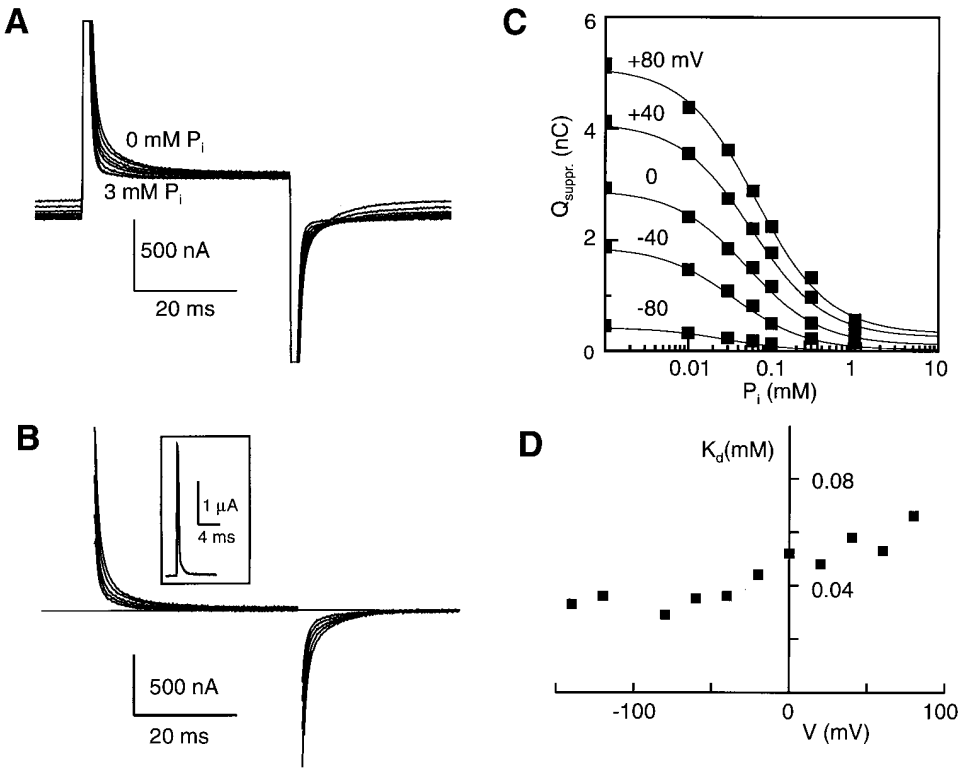

FIGURE 7. The effect of changing external P_i on pre–steady state relaxations. (*A*) Pre–steady state relaxations recorded from a cell expressing NaP_i-2 for a voltage jump from −100 to 0 mV for 0, 0.01, 0.03, 0.06, 0.1, 0.3, 1, and 3.0 mM P_i. The initial baseline shift reflects the steady state holding current induced by each P_i. P_i was applied in increasing concentration. Between successive applications, the cell was allowed to recover in 0 mM P_i until the initial steady state holding current at −50 mV was reestablished. (*B*) The P_i-suppressed current obtained by subtracting the record at 3 mM P_i from the test record under the same voltage step conditions as *A* and same cell. Each trace has been baseline-adjusted to the steady state value. The first millisecond of each difference record during the voltage transition was blanked. This corresponds to the time to complete most of the oocyte capacitive charging as indicated in the inset for a voltage jump from −50 to −40 mV, plotted on the same time scale (same cell). (*C*) P_i dose response for the same cell showing amount of apparent charge suppressed ($Q_{suppr.}$) at −100 mV as a function of P_i for five target potentials as indicated. Charge was estimated by numerical integration of the records as in *B*, with the steady state holding current suppressed. A small error is expected in $Q_{suppr.}$ due to starting the integration at 1 ms. Continuous lines show fits with Eq. 1 for $n = -1$. (*D*) Voltage dependence of apparent K_d for suppression of pre–steady state charge found from fitting Eq. 1 to the data, for the same cell as in *C*.

function of the target potential (Fig. 7 *D*). This indicated that the P_i concentration required to suppress 50% of the available charge at $V_h = -100$ mV was relatively voltage independent.

Dependence on pH. H^+ ions might also contribute to the pre–steady state relaxations since, for some Na^+-coupled cotransporters, they are also known to act as a substrate (e.g., Hirayama et al., 1994). To test this hypothesis, we first investigated the effect of varying pH on pre–steady state relaxations with 96 mM Na^+. As shown in Fig. 8 *A* for voltage steps to three test potentials, a reduction in external pH from 7.4 to 6.2 caused a clear suppression of the relaxations both for the ON and OFF transitions, and the corresponding reduction in I_p was 81%. Quantification of the relaxations by single exponential curve fitting to the main relaxation revealed a consistent change in the relaxation voltage dependence as pH was reduced from 7.4 to 6.2: $V_{0.5}$ of the Q-V curve shifted towards depolarizing potentials (Fig. 8 *B*) and the relaxations slowed significantly for $V > 0$ in the τ-V data (Fig. 8 *C*). As shown in Fig. 8 *D*, when Na^+ was removed from the external medium changing pH from 7.4 to 6.2 further suppressed the relaxations; however, their small magnitude under these conditions prevented further quantification. No P_i-induced transport was detected in the steady state in the absence of external Na^+ at these pH values (data not shown).

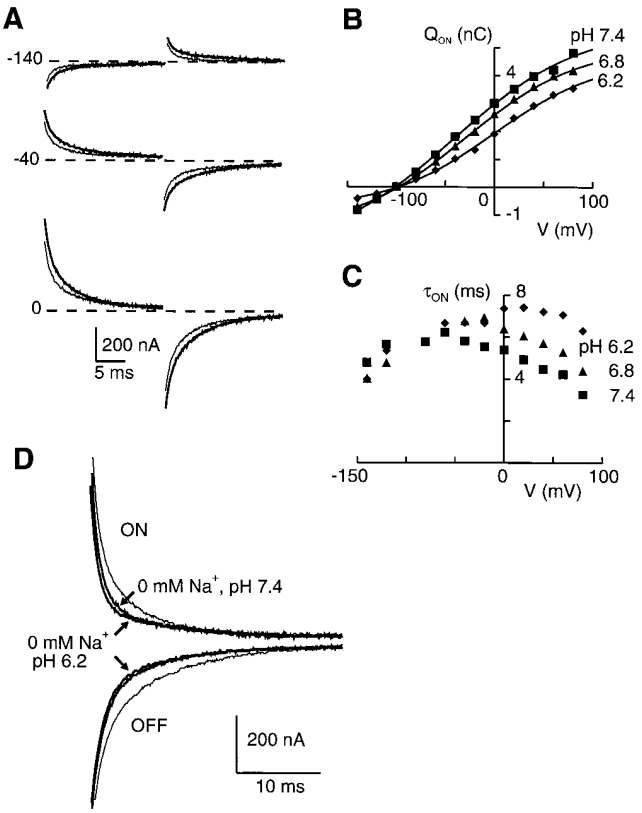

FIGURE 8. The effect of external pH on pre–steady state relaxations. (*A*) Superimposed pre–steady state relaxations for ON and OFF voltage steps to the test potentials indicated from a holding potential of −100 mV for the same cell with 96 mM Na^+ in external medium. Thick traces, pH 7.4; thin traces, pH 6.2. To suppress the endogenous capacitive transient, the records were blanked for the first 3 ms after the transition. (*B*) Apparent charge movement for three pHs indicated in the presence of 96 mM Na^+. Continuous lines are fits using the Boltzmann function (Eq. 2). The fit parameters were: (pH 7.4) $z = 0.38$, $V_{0.5} = -40$ mV, $Q_{max} = 7.4$ nC; (pH 6.8) $z = 0.37$, $V_{0.5} = -23$ mV, $Q_{max} = 7.5$ nC; (pH 6.2) $z = 0.46$, $V_{0.5} = -2$ mV, $Q_{max} = 5.3$ nC. (*C*) Voltage dependence of main ON relaxation τ for three pHs indicated and the same cell as in *B*. (*D*) Pre–steady state relaxations recorded from another cell for a step from −100 to 0 mV (ON) and returning to −100 mV (OFF) for three superfusion conditions: 96 mM Na^+, pH 7.4 (*thin trace*); 0 mM Na^+, pH 7.4, and 0 mM Na^+, pH 6.2 (*arrows*). The graphical superposition of the traces reveals that after removal of Na^+ from the external medium, a reduction in pH leads to a further suppression of the relaxations. To suppress the endogenous capacitive transient, the records are blanked for the first 3 ms after the transition.

DISCUSSION

Steady State Behavior

Comparison with previous results. Our characterization of the steady state kinetics of the rat Na^+/P_i cotransporter isoform, NaP_i-2, gave findings consistent with those reported in previous electrophysiological studies (Busch et al., 1994, 1995; Hartmann et al., 1995). In these studies, kinetic parameters were determined over a limited potential range and no definitive conclusions regarding the voltage dependence of kinetics could be drawn. At $V_h = -50$ mV, we consistently measured a sixfold lower K_m^{Pi} compared with the value (0.31 mM) previously reported by Busch et al. (1994). The reason for this is unclear, although subsequent papers by this group characterizing other mammalian isoforms have also reported lower K_m^{Pi} (Busch et al., 1995; Hartmann et al., 1995), in agreement with our present findings. For both isotope flux and electrophysiological measurements, a Hill coefficient of unity at neutral pH for the P_i dose response is a consistent finding, providing strong evidence for a 1:1 stoichiometry for P_i. In the present case, we observed a Hill coefficient <1 at 50 mM Na^+, which may reflect a systematic error in estimating I_p at levels close to or smaller than the endogenous oocyte currents.

Despite the lack of saturation of the Na^+ dose response, our estimate for K_m^{Na} lies within the range also reported for BBMV flux assays (Hoffmann et al., 1976), where larger Na^+ concentrations could be used, and previous electrophysiological studies on oocytes (Busch et al., 1994, 1995). However, in contrast to previous findings on BBMVs, we found that K_m^{Na} was dependent on P_i (Gmaj and Murer, 1986; see also Béliveau and Strévey, 1988). Furthermore, from BBMV studies, the

Hill coefficient for Na^+ binding was generally taken to be around 2, whereas the estimates we obtained, consistent with those previously reported for NaP_i-2 (Busch et al., 1994), indicated a Hill coefficient significantly >2. These discrepancies might be due to inherent differences between the cloned transporter expressed in *Xenopus* oocytes and the native form in BBMVs, as well as possible contamination from type I Na^+/P_i cotransporters in the latter case. We previously reported (Forster et al., 1997*a*) a Hill coefficient for apparent Na^+ binding significantly <2 for the flounder type II isoform (NaP_i-5) even though the K_m^{Na} was close to that for NaP_i-2. This may reflect real differences in the steady state kinetics of these two isoforms: for example, the larger Hill coefficient for NaP_i-2 might indicate a greater degree of cooperativity for Na^+ binding (Weiss, 1997). However, a rigorous determination of the stoichiometry can only be undertaken by measuring the substrate uptake and electrogenic properties on the same oocyte (e.g., Eskandari et al., 1997). Moreover, the use of the Hill equation to infer a stoichiometry of the substrate binding should be approached with caution (Weiss, 1997) and the finding of an apparent 3:1 stoichiometry in the case of NaP_i-2, although attractive, should be conservatively taken as a lower limit.

Order of substrate binding. Two limitations of the intact oocyte preparation for studying cotransport function restrict the information obtained from steady state dose-response measurements: (*a*) there is no direct control of *trans* substrate concentrations, and (*b*) the normal osmolarity of ~200 mosM places an upper limit on the usable substrate concentrations, particularly in the case of Na^+, where we were only able to measure the kinetics just above the predicted K_m^{Na}. Given these limitations, we can nevertheless draw tentative conclusions about the order of substrate binding on the *cis* face. For P_i as the variable substrate, both "V" and "K" kinetics are found, where V kinetics refers to a maximum transport rate dependency on the fixed substrate and K kinetics refers to an apparent affinity constant dependency on the fixed substrate (e.g., Stein, 1990). This is indicated here by the dependency of both I_{pmax} and K_m^{Pi} on Na^+. With K kinetics alone, random binding schemes can most likely be excluded, such as proposed by Béliveau and Strévey (1988) for Na^+/P_i cotransport in BBMVs. Furthermore, having V kinetics for the P_i dose dependency would be consistent with either P_i or Na^+ being the last substrate to bind before translocation. On the other hand, although the maximum Na^+ was 120 mM, our fits to the Na^+ dose-dependency data suggest that only K kinetics are involved in the apparent Na^+ binding. Taken together, this behavior would indicate that Na^+ is the last substrate to bind. Yet, based on the steady state data alone, we cannot exclude the possibility that an additional Na^+ binding step precedes P_i binding, as has been proposed for the Na^+/glucose cotransporter by Restrepo and Kimmich (1985), and Bennett and Kimmich (1992). Our finding of a Na^+-dependent slippage component, which was directly related to the expression level of functional NaP_i-2, also suggested that Na^+ can interact with NaP_i-2 in the absence of P_i (see also Béliveau and Strévey, 1988).

In summary, the steady state data would be consistent with an ordered scheme for substrate binding on the *cis* face as seen in Scheme I, where C_o represents the unloaded carrier oriented towards the *cis* face. Based on the stoichiometry of the slippage component, we assumed a stoichiometry of 1:1 for the first Na^+ binding reaction and that the second Na^+ binding step involved two Na^+ ions to account for the Na^+ stoichiometry estimate of 3:1.

$$C_o \Leftrightarrow C_oNa \Leftrightarrow C_oNa\,P_i \Leftrightarrow C_oNa\,P_i\,Na^2$$

$$\Downarrow \textit{slippage} \qquad\qquad \Downarrow \textit{cotransport}$$

(SCHEME I)

Voltage dependence of substrate binding. The apparent affinity constants for both substrates increased with membrane depolarization, but, as shown in Table III, the relative voltage sensitivity of K_m was itself dependent on the concentration of the fixed substrate. For example, for V in the range −100 to 0 mV, the apparent P_i binding at 96 mM Na^+ increased by 60%, whereas at 50 mM Na^+ it increased more than threefold. In contrast, the relative voltage dependence of K_m^{Na} showed <50% increase over a 10-fold range of P_i. These data suggest that the apparent binding of Na^+, rather than P_i, is a determinant of voltage dependence. This conclusion should be treated with caution since in any analytical expression for the steady state transport expressed in the form of Eq. 1, the apparent K_m will be a function of all the rate constants, including the unloaded carrier. Therefore, the voltage dependence of the apparent affinity for any substrate does not necessarily reflect the voltage dependence of the true affinity constant (Restrepo and Kimmich, 1985; Bennett and Kimmich, 1996).

The effect of slippage on steady state kinetics. The relatively high endogenous current in typical oocytes, compared with the P_i-induced component, necessitated subtraction of the endogenous background current from the total P_i-induced current under the assumptions that (*a*) the background current is only due to endogenous effects, and (*b*) it is P_i insensitive. Our finding of a Na^+-dependent slippage component similar to that first reported by Umbach et al. (1990) for the Na^+/glucose transporter, SGLT1, means that the validity of these assumptions must be reevaluated. The presence of slip-

TABLE III

Substrate Voltage Dependence Normalized to K_m at −100 mV

V (mV)	−80	−60	−40	−20	0
K_m^{Na} (0.1 mM P_i)	1.01	1.08	1.17	1.41	1.48
K_m^{Na} (1.0 mM P_i)	1.00	1.04	1.08	1.21	1.24
K_m^{Pi} (50 mM Na^+)	1.14	1.57	2.08	2.41	3.68
K_m^{Pi} (96 mM Na^+)	1.03	1.14	1.28	1.43	1.59

Data are taken from the absolute apparent affinity constant data for P_i binding and Na^+ binding in Figs. 2 *C* and 3 *C*, respectively.

page could lead to errors in interpreting steady state kinetic data, particularly at saturating P_i. If this component were suppressed in the presence of P_i due to a faster rate constant for the P_i binding step as P_i increases, an underestimate of the true coupled current by ~10% at saturating P_i would result, since both the endogenous component and a NaP_i-2-related component are subtracted from the test response.

Pre–Steady State Kinetics

Pre–steady state relaxations are a common feature of cation-coupled cotransporters that exhibit electrogenicity, being first reported by Birnir et al. (1990) for the cloned Na^+/glucose cotransporter (SGLT1). Subsequent detailed kinetic studies of the SGLT family (e.g., Parent et al., 1992*a*, 1992*b*; Loo et al., 1993; Mackenzie et al., 1996; Hazama et al., 1997) and studies of other Na^+-coupled cotransporters (e.g., Mager et al., 1993; Hager et al., 1995; Wadiche et al., 1995; Eskandari et al., 1997; Forster et al., 1997*a*) have established this technique as an important tool for identification of partial reactions in the transport cycle. In the present case, we have demonstrated that oocytes expressing NaP_i-2 exhibit pre–steady state relaxations with properties qualitatively similar to those previously reported for the flounder isoform, NaP_i-5 (Forster et al., 1997*a*) despite a four- to fivefold lower expression.

Transport turnover. The slope of the $I_{p(-100)}$–$Q_{(-100)}$ relation can be used to estimate the apparent turnover of NaP_i-2 at −100 mV, assuming that (*a*) the charge translocation is a single step having an apparent valence *z*, and (*b*) the same number of transporters contribute to $I_{p(-100)}$ in the presence of saturating P_i, as contribute to translocatable charge ($Q_{(-100)}$) in the absence of P_i. The transporter turnover, ϕ, is then given by:

$$\phi = I_{p(-100)}\, z/Q_{(-100)}. \quad (3)$$

Taking $z \approx 0.5$ from the Boltzmann fit to the Q-V relation and $I_{p(-100)}/Q_{(-100)} = 46\ s^{-1}$, Eq. 3 gives $\phi = 23\ s^{-1}$ at −100 mV and 96 mM Na^+. This is comparable with the estimates of ϕ for other Na^+-coupled transporters expressed in *Xenopus* oocytes under similar conditions, including NaP_i-5 ($35\ s^{-1}$) (Forster et al., 1997*a*).

Voltage-dependent steps. Like NaP_i-5 (Forster et al., 1997*a*), in 0 mM P_i, reducing Na^+ resulted in a negative shift of $V_{0.5}$ for the Q-V distribution without significantly affecting the total charge. However, if the charge movement were solely due to an "ion-well" effect, a much larger change in the voltage dependence of the τ-V relation would be expected (Forster et al., 1997*a*). Moreover, in 0 mM external Na^+, a relaxation was still observed that was only suppressed if both substrates were present at the maximum concentrations used (96 mM Na^+, 3 mM P_i). These findings suggested that (*a*) the unloaded carrier itself contributes significantly to the pre–steady state relaxations, and (*b*) Na^+ is able to bind first, as deduced from the steady state analysis

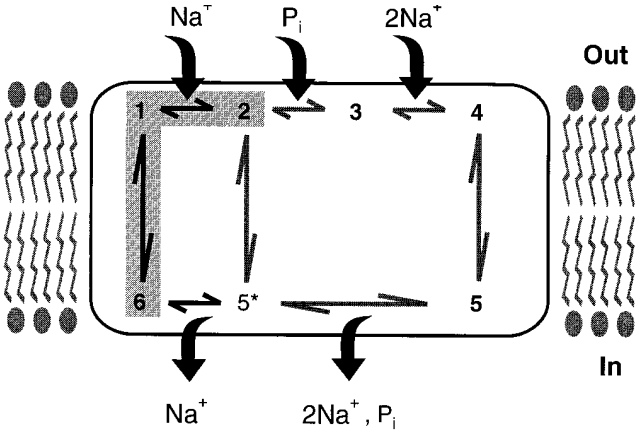

FIGURE 9. A state diagram representation of an ordered binding model for NaP_i-2. Voltage-dependent partial reactions identified by pre–steady state experiments (translocation of the unloaded carrier, 6 ⇔ 1; binding of the first Na^+, 1 ⇔ 2) are shown shaded. The empty cotransporter is assumed to have a valency of −1, but this charge translocates through a fraction of the transmembrane field to account for an apparent valency <1 derived from fits using Eq. 2. Both the slippage (2 ⇔ 5*) pathway and translocation of the fully loaded carrier (4 ⇔ 5) are assumed to be electroneutral. Depending on the availability of substrate and membrane potential, accessibility to the substrate binding sites favors either the *cis* (states 1, 2, 3, 4) or *trans* (states 5, 5*, 6) side of the membrane. Under normal physiological conditions with $V < 0$, the apparent transport cycle proceeds clockwise around the loop. For $V < 0$, and low internal Na^+, external Na^+ binding is facilitated on the *cis* side due to the outward translocation of −ve charge associated with transition 6 ⇔ 1. This allows one Na^+ ion to move to its binding site within the transmembrane field, leading to an increasing of the affinity of the transporter for P_i (assumed to be predominantly divalent at neutral pH), which then binds (2 ⇔ 3) in a voltage-independent manner. Then follows a further voltage-independent step involving the binding of two Na^+ ions (3 ⇔ 4) to give electroneutrality. The fully loaded carrier is now able to translocate (4 ⇔ 5), release substrates on the *trans* side, and return to state 6. A net inward charge movement of +1 electronic units occurs per cycle, which is manifested as I_p. Except for slippage, the order of binding/release of substrates on the cytosolic side cannot be determined using the intact oocyte preparation and, therefore, the cytosolic release of cotransported P_i, together with two Na^+ ions, is lumped as one reaction (5 ⇔ 5*).

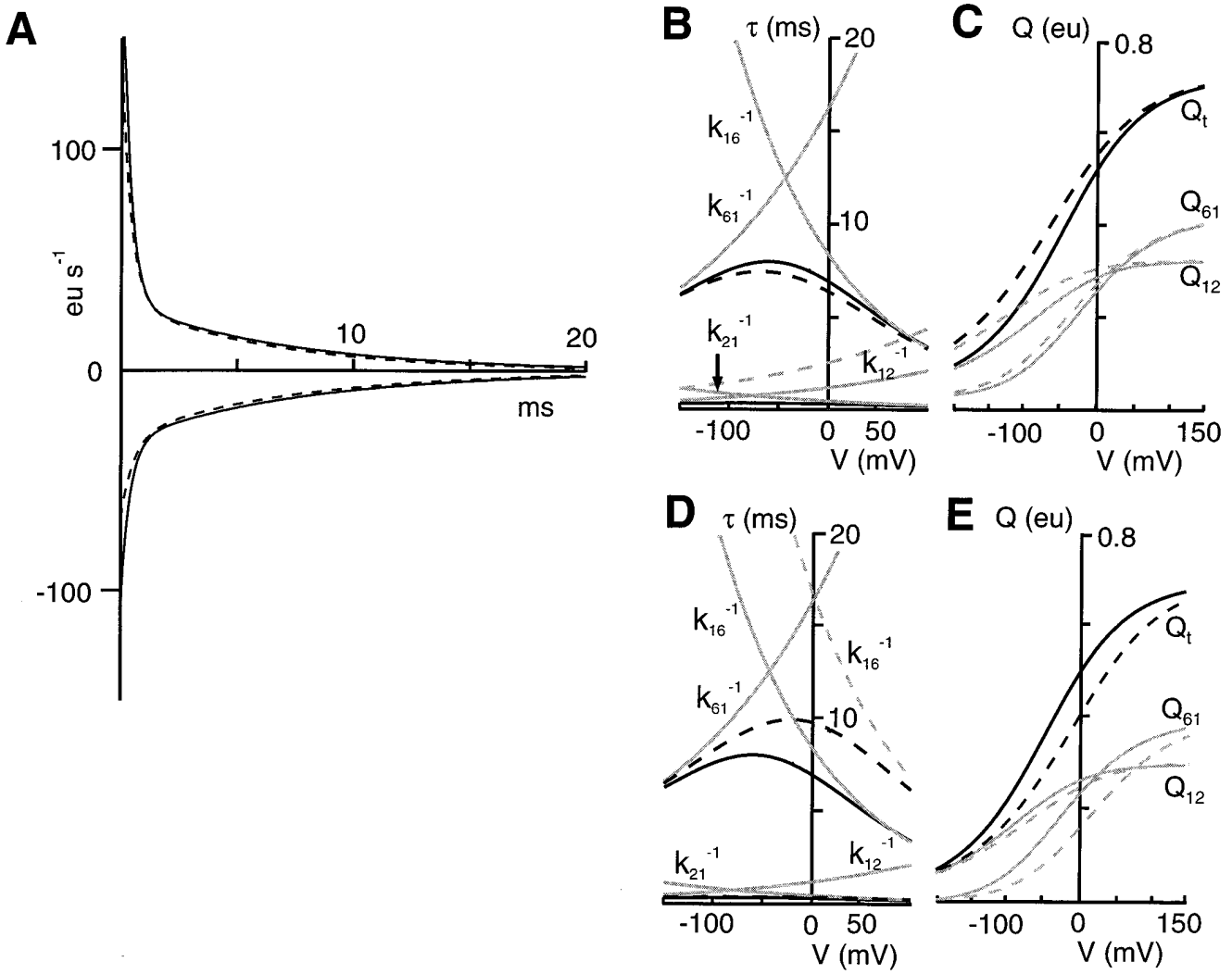

FIGURE 10. Simulations predict voltage-dependent behavior of pre–steady state kinetics in the absence of external P_i. Values were assigned to the parameters associated with voltage-dependent partial reactions (shown shaded in Fig. 9: unloaded carrier, 6 ⇔ 1; first Na^+ binding/debinding, 1 ⇔ 2) to give a reasonable match to the measured τ-V and Q-V data under varying external Na^+. (*A*) Simulations of pre–steady state current showing the ON and OFF relaxations for a step from −100 to 0 mV for two external Na^+ concentrations (*continuous lines*, 100 mM; *broken lines*, 50 mM). The voltage step is assumed to occur instantaneously so that no account is taken of the speed of oocyte membrane charging. Note that because of the voltage dependence of k_{21}, the fast component in the relaxation appears more prominent in the ON than OFF traces for both Na^+, and this can lead to significant errors in estimating Q_{ON} and Q_{OFF} (see DISCUSSION). Rate constants for voltage dependent steps are (s^{-1}): $k_{61} = 60 \exp(-0.16\ eV/kT)$, $k_{16} = 120 \exp(0.24\ eV/kT)$, $k_{12} = 8{,}000\ [Na] \exp(-0.15\ eV/kT)$, $k_{21} = 2{,}000 \exp(0.15\ eV/kT)$, where [Na] = Na^+ concentration (Molar). The corresponding valences and asymmetry factors are: $z_{61} = 0.4$, $z_{12} = 0.5$, $\delta_{61} = 0.4$, $\delta_{12} = 0.5$. Ordinate scale is in electronic units (*eu*) s^{-1}, where 1 eu = 1.602×10^{-19} C. (*B*) Simulated τ-V relations for two external Na^+ concentrations as in *A*. Bold curves represent the two nonzero time constants predicted from the eigenvalue solutions of the three-state model involving transitions 6 ⇔ 1 and 1 ⇔ 2 (*continuous curves*, 100 mM; *broken curves*, 50 mM). The faster component with τ < 1 ms would not be detected easily by curve fitting due to the oocyte charging transient. Light curves represent the voltage dependence of the reciprocal rate constants for the transitions indicated by the respective subscripts. Note that only k_{12} is dependent on Na^+. (*C*) Simulated steady state Q-V relation for the same two Na^+ concentrations. The amount of charge in electronic units contributed by the two transitions is shown (Q_{61}, Q_{12}), together with the total charge (Q_t). For the simulation, the holding potential was set at −1,000 mV to obtain normalized relations. Fitting Eq. 2 to the Q_t-V data predicted $z = 0.5$ and a shift of −16 mV for a change in Na^+ from 100 to 50 mM. (*D*) Simulation of the effect of pH on pre–steady state kinetics. The unloaded carrier backward rate constant (K_{16}) is assumed to be decreased from 120 to 60 s^{-1}, resulting from an increase in external H^+ as indicated by measurements. The τ-V curves predict an increase of the slower relaxation for V > 0. Continuous lines represent τs (*bold*) and inverse rate constants (*light*) under normal (pH 7.4) conditions. Broken lines are for reduced pH conditions. (*E*) The corresponding steady state Q-V relations for the same change in rate constant K_{16} showing the shift in the Q-V distribution towards depolarizing potentials (*broken lines*) resulting primarily from a shift in the steady state charge distribution of the unloaded carrier.

since, in the alternative binding scheme $C_o \Leftrightarrow C_oP_i \Leftrightarrow C_oP_iNa$, no Na^+-dependent influence on the steady state charge distribution would be expected with 0 mM P_i.

For P_i as the variable substrate, pre–steady state relaxations were also suppressed in a dose-dependent manner, but fitting to a single Boltzmann function showed no significant shift in $V_{0.5}$ and only a weak voltage dependence of the apparent K_d for charge suppression, similar to the weak voltage dependence of K_m^{Pi} at 96 mM Na^+. In agreement with our steady state findings, these results suggested that the apparent P_i binding did not directly contribute to charge movements; i.e., the P_i binding site lies outside the transmembrane electric field.

A characteristic feature of type II Na^+/P_i cotransport is its dependence on external pH, whereby H^+ ions are thought to compete for occupancy of the Na^+ binding site, thereby increasing the apparent K_m^{Na} (Amstutz et al., 1985). Our finding of a shift of $V_{0.5}$ for the Q-V curve towards depolarizing potentials and a positive shift in the peak of the τ-V data does not accord with the simple notion of H^+ ions either competing for occupancy of the Na^+ binding site and/or reducing the effective Na^+ concentration as seen by the first Na^+ binding site (i.e., ion-well). One candidate mechanism could involve the interaction of H^+ ions with the empty carrier. This is supported by our observation that, at 0 mM Na^+, the relaxations were also suppressed for a change in pH from 7.4 to 6.2, and findings from a recent study of the flounder isoform NaP_i-5, where higher resolution recordings were possible (Forster et al., 1997*b*).

An Ordered Kinetic Model for NaP_i-2

Fig. 9 depicts the state diagram for a model that can account for the kinetic properties we have deduced for NaP_i-2. This scheme is derived from that proposed for the cloned Na^+/glucose cotransporter (SGLT1) by Parent et al. (1992*b*), but includes a second Na^+ binding step to account for the dependence of I_{pmax} on Na^+ in the steady state. Restrepo and Kimmich (1985) and Bennett and Kimmich (1996) have proposed a similar scheme, which also includes a second Na^+ binding step, to describe Na^+/glucose cotransport characterized in LLC-PK1 epithelia cells. To simplify the model, we assumed the binding of the two Na^+ ions (step 3 ⇔ 4) occurs with strong positive cooperativity to give an apparent simultaneous binding (Falk et al., 1998; Weiss, 1997). As for P_i binding (step 2 ⇔ 3), this is assumed to occur external to the transmembrane field, so that it does not contribute to pre–steady state charge movements with finite P_i. With the two voltage-dependent steps identified from the pre–steady state data (6 ⇔ 1 and 1 ⇔ 2), the model successfully accounts for a num-

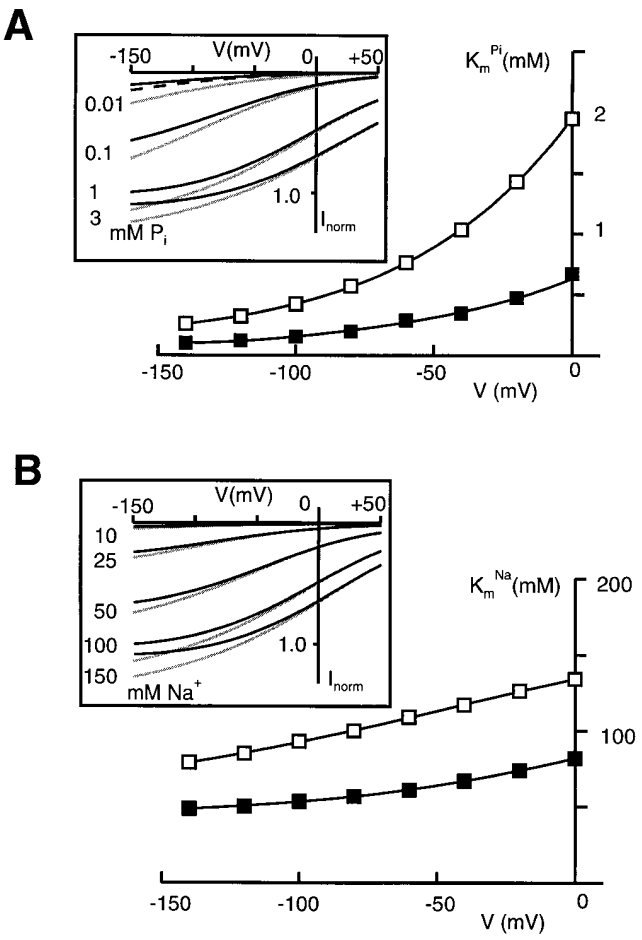

FIGURE 11. Simulations of P_i-induced currents in the steady state, assuming zero *trans* conditions. Since the transition 6 ⇔ 1 is the only translocation step involving net charge movement, the steady state current is proportional to $X_1k_{16} - X_6k_{61}$, where X_1 and X_6 are the occupancy of states 1 and 6, respectively. Voltage-dependent rate constants and parameters are given in Fig. 10. Additional rate constants for the kinetic scheme of Fig. 9 are (s^{-1}): $k_{23} = 1{,}000$ $[P_i]$, $k_{32} = 100$, $k_{34} = 500$ $[Na]^2$, $k_{43} = 50$, $k_{45} = k_{54} = 25$, $k_{55*} = 10{,}000$, $k_{5*5} = 0$, $k_{5*6} = 10{,}000$, $k_{65*} = 0$, $k_{25*} = 2.5$, $k_{5*2} = 2.5$, where $[P_i]$ and [Na] are the concentrations of P_i and Na^+, respectively (Molar). These were chosen to give reasonable predictions of the experimentally observed I-V relations. (*A*) P_i dose response. Inset shows a set of I-V curves for nominal P_i values indicated, normalized to I_p at −100 mV. Dashed curve is the slippage component (simulated with $P_i = 0$ mM), light curves represent the total simulated P_i-induced steady state current and bold curves represent the steady state response with slippage component subtracted (equivalent to the P_i-induced response measured). Eq. 1 was fit to the data to obtain the apparent K_m^{Pi} as a function of V for nominal 100 (■) and 50 (□) mM Na^+. The continuous lines are for visualization only. (*B*) Na^+ dose response. (*inset*) Set of I-V curves for nominal Na^+ values indicated, and 1 mM nominal P_i, normalized to I_p at −100 mV. Light curves represent the simulated total steady state current, bold curves have slippage component subtracted (equivalent to the P_i-induced response measured). Eq. 1 was fit to the data to derive the apparent K_m^{Na} as a function of V for nominal 1 (■) and 0.1 (□) mM P_i. The continuous lines are for visualization only.

ber of the features observed in both the pre–steady state and steady state.

Two pre–steady state components. Fig. 10 *A* shows simulated pre–steady state relaxations induced by a voltage step for two nominal Na^+ concentrations (50 and 100 mM) in the absence of P_i. The corresponding τ-V and Q-V curves are shown in Fig. 10, *B* and *C*, respectively. As predicted from a three-state model, the total relaxation comprises two components that are visible in the simulation. In practice, because the fast component has a τ comparable with that of the intrinsic oocyte charging, its detection would be difficult with biexponential fitting to the total relaxation. Moreover, the inherent low-pass filtering by the passive membrane would further distort this component (Forster and Greeff, 1992). We obtained evidence for the second component by subtraction of the transient under saturating conditions (3 mM P_i, 96 mM Na^+), whereby we assumed that all endogenous relaxations were fully suppressed. Further characterization of the fast component would require the cut-open oocyte technique (e.g., Chen et al., 1996) to improve the recording bandwidth and rise time.

Voltage dependence of τ-V and Q-V relations. For a reduction in external Na^+, our data suggested that the main ON τ became slightly faster. With the translocation of the empty carrier ($6 \Leftrightarrow 1$) as the rate limiting voltage-dependent step and external Na^+ debinding faster than binding (i.e., $k_{21} > k_{12}$), the simulation also predicts a small downward shift in the τ-V curve as external Na^+ is reduced. Moreover, the Na^+-dependent shift of $V_{0.5}$ for the ON Q-V distribution is also predicted by the model. Note that as the steady state charge distributions of both components are influenced by external Na^+ (Fig. 10 *C*), a shift in $V_{0.5}$ would still be expected even if the fast component were not detected by single exponential curve fitting.

Charge imbalance in total relaxation. Our inability to detect the faster component in the complete relaxation can account for the charge imbalance of the apparent ON and OFF charge estimated from single exponential curve fitting. The voltage dependence of the fast component means that for depolarizing (ON) steps from $V_h = -100$ mV, single exponential fits commencing after the capacitive transient will accurately detect the slower component. However, for the corresponding OFF step, the fitted record now includes part of the fast component, thus giving a larger apparent charge for the OFF transition. The converse would apply for steps from a more positive V_h, since the ON charge transfer results from a hyperpolarizing step. The good agreement between Q_{ON} and Q_{OFF}, by integrating the charge remaining after subtraction of the relaxation with saturating P_i, also supports this interpretation.

pH effects. We found the observed changes in the τ-V and Q-V could be simulated by assuming that H^+ ions interact with the unloaded transporter to cause a reduction of the rate constant K_{16}. The τ-V relation (Fig. 10 *D*) shows the observed slowing of the main relaxation for depolarized potentials, and the corresponding Q-V curve (Fig. 10 *E*) predicts a positive shift in the steady state charge distribution as we observed.

Steady state behavior. For the P_i dose dependency (Fig. 11 *A, inset*), the predicted I-V curves indicate rate limiting behavior at extremes of membrane voltage and saturation at high P_i as observed experimentally. Furthermore, at hyperpolarizing potentials, the subtraction procedure used to obtain the apparent P_i-induced current results in more pronounced rate limiting behavior due to the subtraction of the slippage component present in the control (0 mM P_i) response. Fitting Eq. 1 to the simulated data gave a voltage-independent Hill coefficient ≈ 1 that was independent of Na^+ (data not shown) and an apparent K_m^{Pi} (Fig. 11 *A*) that increased monotonically with depolarizing voltage and was sensitive to Na^+. For the Na^+ dose response, the simulated I-V curves (Fig. 11 *B, inset*) are also qualitatively similar to the experimental data whereby, after subtraction of the response at 0 mM P_i, the Hill coefficient predicted from fitting Eq. 1 to the simulated I-V data was 2.4 and the apparent K_m^{Na} varied weakly with potential for a 10-fold change in P_i (Fig. 11 *B*).

The authors acknowledge the helpful comments and critical reading of the manuscript by Prof. E. Wright and Dr. Don Loo.

This work was supported by grants to H. Murer from the Swiss National Science Foundation (SNF: 31-46523), the Hartmann Müller-Stiftung (Zurich, Switzerland), the Olgar Mayenfisch-Stiftung (Zurich), and the Schweizerischer Bankgesellschaft (Zurich) (Bu 704/7-1).

Original version received 19 February 1998 and accepted version received 4 May 1998.

REFERENCES

Adrian, R.H. 1978. Charge movement in the membrane of striated muscle. *Annu. Rev. Biophys. Bioeng.* 7:85–112.

Amstutz, M., M. Mohrmann, P. Gmaj, and H. Murer. 1985. Effect of pH on phosphate transport in rat renal brush border vesicles. *Am. J. Physiol.* 248:F705–F710.

Bennett, E., and G.S. Kimmich. 1992. Na^+ binding to the Na^+-glucose cotransporter is potential dependent. *Am. J. Physiol.* 262:C510–C516.

Bennett, E., and G.S. Kimmich. 1996. The molecular mechanism and potential dependence of the Na+/glucose cotransporter. *Biophys. J.* 70:1676–1688.

Béliveau, R., and H. Ibnoul-Khatib. 1988. Electrogenicity of phosphate transport by renal brush-border membranes. *Biochem. J.* 252:801–806.

Béliveau, R., and J. Strévey. 1991. Phosphate transport in kidneys: effect of transmembrane electrical potential. *Am. J. Physiol.* 261: F663–F669.

Béliveau, R., and J. Strévey. 1988. Kinetic model for phosphate transport in renal brush-border membranes. *Am. J. Physiol.* 249: F329–F336.

Bertrand, D., and Ch. Bader. 1986. DATAC: a multipurpose biological data analysis program based on a mathematical interpreter. *Int. J. Biomed. Comput.* 18:193–202.

Birnir, B., D.D.F. Loo, and E.M. Wright. 1990. Voltage-clamp studies of the Na^+/glucose cotransporter cloned from rabbit small intestine. *Pflügers Arch.* 418:78–95.

Burckhardt, G., H. Stern, and H. Murer. 1981. The influence of pH on phosphate transport into rat renal brush border membrane vesicles. *Pflügers Arch.* 390:191–197.

Busch, A.E., S. Waldegger, T. Herzer, J. Biber, D. Markovich, G. Hayes, H. Murer, and F. Lang. 1994. Electrophysiological analysis of Na^+/P_i cotransport mediated by a transporter cloned from rat kidney in *Xenopus* oocytes. *Proc. Natl. Acad. Sci. USA.* 91:8205–8208.

Busch, A.E., C.A. Wagner, A. Schuster, S. Waldegger, J. Biber, H. Murer, and F. Lang. 1995. Properties of electrogenic P_i transport by NaP_i-3, a human renal brush border Na^+/P_i transporter. *J. Am. Soc. Nephrol.* 6:1547–1551.

Chen, X.Z, M.J. Coady, and J.-Y. Lapointe. 1996. Fast voltage clamp discloses a new component of pre–steady state currents from the Na^+-glucose cotransporter. *Biophys. J.* 71:2544–2552.

Eskandari, S., D.D.F. Loo, G. Dai, O. Levy, E.M. Wright, and N. Carrasco. 1997. Thyroid Na^+/I^- symporter. *J. Biol. Chem.* 43: 27230–27238.

Falk, S., A. Guay, C. Chenu, S.D. Patil, and A. Berteloot. 1998. Reduction of an eight-state mechanism of cotransport to a six-state model using a new computer program. *Biophys. J.* 74:816–830.

Forster, I.C., and N.G. Greeff. 1992. The early phase of sodium channel gating current in the squid giant axon. *Eur. Biophys. J.* 21:99–116.

Forster, I., A.E. Busch, F. Lang, J. Biber, and H. Murer. 1996. Characteristics of the steady state voltage dependence of the rat renal type II Na/P_i cotransporter (NaP_i-2). *J. Am. Soc. Nephrol.* 7:*A*2769. (Abstr.)

Forster, I.C., C.A. Wagner, A.E. Busch, F. Lang, J. Biber, N. Hernando, H. Murer, and A. Werner. 1997*a*. Electrophysiological characterization of the flounder type II Na^+/P_i cotransporter (NaP_i-5) expressed in *Xenopus laevis* oocytes. *J. Membr. Biol.* 160:9–25.

Forster, I.C., J. Biber, and H. Murer. 1997*b*. Modulation of the voltage-dependent kinetics of renal type II Na^+/P_i cotransporters by external pH. *J. Am. Soc. Nephrol.* 8:*A*2611. (Abstr.)

Gmaj, P., and H. Murer. 1986. Cellular mechanisms of inorganic phosphate transport in kidney. *Physiol. Rev.* 66:36–69.

Hager, K., A. Hazama, H.M. Kwon, D.D.F. Loo, J.S. Handler, and E.M.Wright. 1995. Kinetics and specificity of the renal Na^+/*myo*-inositol cotransporter expressed in *Xenopus* oocytes. *J. Membr. Biol.* 143:103–113.

Hartmann, C.M., C.A. Wagner, A.E. Busch, D. Markovich, J. Biber, F. Lang, and H. Murer. 1995. Transport characteristics of a murine renal Na/P_i-cotransporter. *Pflügers Arch.* 430:830–836.

Hazama, A., D.D.F. Loo, and E.M. Wright. 1997. Presteady-state currents of the Na^+/glucose cotransporter (SGLT1). *J. Membr. Biol.* 155:175–186.

Hirayama, B.A., D.D.F. Loo, and E.M. Wright. 1994. Protons drive sugar transport through the Na^+/glucose cotransporter (SGLT1). *J. Biol. Chem.* 269:21407–21410.

Hoffmann, N., M. Thees, and R. Kinne. 1976. Phosphate transport by isolated renal bush border vesicles. *Pflügers Arch.* 362:147–156.

Holmgren, M., and R.F. Rakowski. 1994. Pre-steady-state transient currents mediated by the Na/K pump in internally perfused *Xenopus* oocytes. *Biophys. J.* 66:912–922.

Kempson, S.A. 1988. Novel specific inhibitors of epithelial phosphate transport. *NIPS (News Physiol. Sci.).* 3:154–157.

Loo, D.D.F., A. Hazama, S. Supplisson, E. Turk, and E.M. Wright. 1993. Relaxation kinetics of the Na^+/glucose cotransporter. *Proc. Natl. Acad. Sci. USA.* 90:5767–5771.

Mager, S., J. Naeve, M. Quick, C. Labarca, N. Davidson, and H.A. Lester. 1993. Steady states, charge movements, and rates for a clones GABA transporter expressed in *Xenopus* oocytes. *Neuron.* 10:177–188.

Mackenzie, B., D.D.F. Loo, M. Panayotova-Heiermann, and E.M. Wright. 1996. Biophysical characteristics of the pig kidney Na^+/glucose cotransporter SGLT2 reveal a common mechanism for SGLT1 and SGLT2. *J. Biol. Chem.* 271:32678–32683.

Murer, H., and J. Biber. 1997. A molecular view of proximal tubular inorganic phosphate (P_i) reabsorption and of its regulation. *Pflügers Arch.* 433:379–389.

Murer, H., D. Markovich, and J. Biber. 1994. Renal and small intestinal sodium-dependent symporters of phosphate and sulphate. *J. Exp. Biol.* 196:167–181.

Murer, H., A. Werner, S. Reshkin, F. Wuarin, and J. Biber. 1991. Cellular mechanisms in proximal tubular reabsorption of inorganic phosphate. *Am. J. Physiol.* 260:C885–C899.

Parent, L., S. Supplisson, D.D.F. Loo, and E.M. Wright. 1992*a*. Electrogenic properties of the cloned Na+/Glucose cotransporter: I. Voltage clamp studies. *J. Membr. Biol.* 125:49–62.

Parent, L., S. Supplisson, D.D.F. Loo, and E.M. Wright. 1992*b*. Electrogenic properties of the cloned Na+/glucose cotransporter: II. A transport model under nonrapid equilibrium conditions. *J. Membr. Biol.* 125:63–79.

Press, W.H., F.P. Flannery, S.A. Teukolsky, and W.T. Vetterling. 1992. Numerical recipes in C. Cambridge University Press, Cambridge, United Kingdom. 382–397.

Restrepo, D., and G.A. Kimmich. 1985. Kinetic analysis of mechanism of intestinal Na^+-dependent sugar transport. *Am. J. Physiol.* 248:C498–C509.

Samarzija, I., V. Molnar, and E. Frömter. 1980. The stoichiometry of Na^+ coupled anion absorption across the brush border membrane of rat renal proximal tubule. *Proc. 28th Int. Congr. Physiol. Sci.* (Abstr.).

Stein, W.D. 1990. Channels, carriers and pumps. Academic Press Inc., San Diego, CA. 173–219.

Umbach, J.A., M.J. Coady, and E.M. Wright. 1990. Intestinal Na^+/glucose cotransporter expressed in *Xenopus* oocytes is electrogenic. *Biophys. J.* 57:1217–1224.

Wadiche, J.I., J.L. Arriza, S.G. Amara, and M.P. Kavanaugh. 1995. Kinetics of a human glutamate transporter. *Neuron.* 14:1019–1027.

Weiss, J.N. 1997. The Hill equation revisited: uses and misuses. *FASEB J.* 11:835–841.

Werner, A., J. Biber, J. Forgo, M. Palancin, and H. Murer. 1990. Expression of renal transport systems for inorganic phosphate and sulfate in *Xenopus laevis* oocytes. *J. Biol. Chem.* 265:12331–12336.